Stiffness and tension gradients of the hair cell's tip-link complex in the mammalian cochlea.

Mélanie Tobin[1,2], Atitheb Chaiyasitdhi[1,2,†], Vincent Michel[2,3,4,†], Nicolas Michalski[2,3,4], Pascal Martin[1,2,*]

[1] Laboratoire Physico-Chimie Curie, Institut Curie, PSL Research University, CNRS, UMR168, F-75248 Paris, France.

[2] Sorbonne Université, F-75252 Paris, France

[3] Laboratoire de Génétique et Physiologie de l'Audition, Institut Pasteur, Paris, France.

[4] UMRS 1120, Institut National de la Santé et de la Recherche Médicale (INSERM), Paris, France.

[†] Equal contribution.

[*] Correspondence: pascal.martin@curie.fr

SIGNIFICANCE STATEMENT: The tip-link complex of the hair cell is mechanically tuned along the tonotopic axis of the cochlea.

ABSTRACT Frequency analysis of sound by the cochlea relies on sharp frequency tuning of mechanosensory hair cells along a tonotopic axis. To clarify the underlying biophysical mechanism, we have investigated the micromechanical properties of the hair cell's mechanoreceptive hair bundle in the rat cochlea. We studied both inner and outer hair cells, which send nervous signals to the brain and amplify cochlear vibrations, respectively. We find that tonotopy is associated with gradients of stiffness and resting mechanical tension, with steeper gradients for outer hair cells, emphasizing the division of labor between the two hair-cell types. We demonstrate that tension in the tip links that convey force to the mechano-electrical transduction channels increases at reduced Ca^{2+}. Finally, we reveal tonotopic gradients in stiffness and tension at the level of a single tip link. We conclude that mechanical gradients of the tip-link complex may help specify the characteristic frequency of the hair cell.

INTRODUCTION

The cochlea –the auditory organ of the inner ear– is endowed with a few thousands of mechanosensory hair cells that are each tuned to detect a characteristic sound frequency (Fettiplace and Kim, 2014). Different frequencies are detected by different cells, which are spatially distributed in the organ according to a frequency –or tonotopic– map (Lewis et al., 1982; Greenwood, 1990; Viberg and Canlon, 2004). Despite its critical importance for frequency analysis of complex sound stimuli, determining the mechanism that specifies the characteristic frequency of a given hair cell remains a major challenge of auditory physiology.

Although certainly not the only determinant of hair-cell tuning (Fettiplace and Fuchs, 1999), we focus here on the contribution of the hair bundle, the cohesive tuft of cylindrical processes called stereocilia that protrude from the apical surface of each hair cell. The hair bundle works as the mechanical antenna of the hair cell (Hudspeth, 1989). Sound evokes hair-bundle deflections, which modulate the extension of elastic elements –the gating springs– connected to mechanosensitive ion channels. By changing the elastic energy stored in the gating springs, sound stimuli affect the channels' open probability, resulting in a mechano-electrical transduction current. Importantly, mechanical stress is conveyed to the mechano-electrical transduction channels by oblique proteinaceous tip links (Pickles et al., 1984; Kazmierczak et al., 2007) that interconnect the stereocilia near their tips. Whether or not the tip link embodies the gating spring, however, is unsure. Electron microscopy (Kachar et al., 2000) and molecular dynamics simulations (Sotomayor et al., 2010) have suggested that the tip link may be too rigid and thus that a compliant element in series with the tip link could determine the gating-spring stiffness. If so (but see (Bartsch et al., 2018)), the gating spring could reside within the assemblies of molecules that anchor both sides of the tip link to the actin core of the stereocilia (Michalski and Petit, 2015), or perhaps be associated with membrane deformations at the lower insertion point of the tip link (Powers et al., 2012). In the following, the molecular assembly comprising the tip link, the transduction channels, as well as the molecules to which they are mechanically connected will be called the 'tip-link complex'.

The operating point of the transducer lies within the steep region of the sigmoidal relation between the transduction current and the hair-bundle position (Corey and Hudspeth, 1983; Russell and Sellick, 1983; Johnson et al., 2011). This key condition for sensitive hearing is thought to be controlled by tension in the tip links at rest (Hudspeth and Gillespie, 1994; Gillespie and Muller, 2009), as well as by extracellular and intracellular calcium (Corey and

Hudspeth, 1983; Ricci et al., 1998; Fettiplace and Kim, 2014), which is thought to stabilize the closed state of the transduction channels (Hacohen et al., 1989; Cheung and Corey, 2006). Tip-link tension has been estimated at ~8 pN in the bullfrog's sacculus (Jaramillo and Hudspeth, 1993) but, to our knowledge, there has been no such report in the mammalian cochlea.

Adaptation continuously resets the mechanosensitive channels to a sensitive operating point when static deflections of the hair bundle threaten to saturate mechanoelectrical transduction (Eatock, 2000). Most of the available evidence indicates that movements by molecular motors actively pulling on the tip links and calcium feedback on the open probability of transduction channels contribute to adaptation. With mammalian cochlear hair cells, however, the dependence of adaptation on Ca^{2+} entry has recently been the subject of significant controversy (Peng et al., 2013; Corns et al., 2014; Peng et al., 2016; Effertz et al., 2017). Motor forces and calcium feedback can also explain the active hair-bundle movements, including spontaneous oscillations, that have been observed in various species (Fettiplace and Hackney, 2006; Martin, 2008). Active hair-bundle motility may contribute to hair-cell tuning by actively filtering and amplifying sound inputs (Hudspeth, 2008). These findings emphasize the importance of the tip-link complex, including the transduction channels, the tip links that convey sound-evoked forces to these channels, as well as the molecular motors that pull on the tip links, for mechanosensitivity of the hair cell.

Electrophysiological properties of the transduction apparatus, including the activation kinetics and the conductance of the transduction channels, as well as the kinetics of adaptation, have been shown to vary with the characteristic frequency of the hair cell (Ricci et al., 2003; Ricci et al., 2005; Fettiplace and Kim, 2014; Beurg et al., 2018). These observations suggest that hair-cell tuning may depend on the transducer itself (Ricci et al., 2005). In addition, it is a ubiquitous property of vertebrate auditory organs that the morphology of the hair bundle varies systematically with the characteristic frequency of the corresponding hair cell (Wright, 1984; Lim, 1986; Roth and Bruns, 1992; Tilney et al., 1992): going from the high-frequency to the low-frequency region of the organ, the hair bundle gets longer and comprises a progressively smaller number of stereocilia. These morphological gradients have long been recognized as circumstantial evidence that the mechanical properties of the hair bundle might be involved in frequency tuning (Turner et al., 1981; Flock and Strelioff, 1984; Fettiplace and Fuchs, 1999). However, a detailed characterization of

mechanical gradients at the level of the whole hair bundle is lacking, in particular to clarify the contribution of the tip-link complex to these gradients.

In this work, we probed passive and active hair-bundle mechanics along the tonotopic axis of an excised preparation of the rat cochlea (Fig. 1). We worked both with inner hair cells, which convey auditory information to the brain and are considered as the true sensors of the organ, and outer hair cells, which are mostly dedicated to cochlear amplification of sound-evoked vibrations (Hudspeth, 2014). We combined fluid-jet stimulation to deflect the hair bundle, iontophoresis of a calcium chelator (EDTA) to disrupt the tip links and measure bundle movements resulting from tension release by these links, and patch-clamp recordings of transduction currents to infer the number of intact tip links contributing to the response. From these measurements, we estimated the stiffness of the whole hair bundle, the contribution of the tip links and of the stereociliary pivots to this stiffness, as well as the resting tension in the tip links. Our results reveal mechanical gradients of the tip-link complex according to the tonotopic map and to the division of labor between sensory inner and amplificatory outer hair cells, providing evidence for the implication of the tip-link complex to frequency tuning of cochlear hair cells.

RESULTS

The hair-bundle stiffness increases along the tonotopic axis. Using a calibrated fluid jet (Methods; Figure 2–figure supplements 1-5), we applied force steps to single hair bundles along the tonotopic axis of the rat cochlea, going from the very apex of the organ to mid-cochlear locations (Fig. 1). Each hair bundle responded to a force step with a fast deflection in the direction of the stimulus followed by a slower movement in the same direction (Fig. 2; Figure 2–figure supplement 5A). Over the duration of the step, the deflection of the hair bundle increased in the direction of the applied step on average by 22% for inner hair cells and by 12% for outer hair cells, corresponding to an apparent softening of the hair bundle by the same amount). A mechanical creep is expected from mechanical relaxation of tip-link tension associated with myosin-based adaptation (Hudspeth, 2014). Accordingly, the creep was strongly reduced upon tip-link disruption by EDTA treatment (Figure 2–figure supplement 5).

For outer hair cells, we found that a given series of force steps evoked hair-bundle deflections that decreased in magnitude towards more basal locations along the tonotopic axis (Fig. 2A). Correspondingly, the slope of a bundle's force-displacement relation (Fig. 2B),

and thus stiffness, increased with the characteristic frequency of the hair cell. The same behavior was observed for inner hair cells (Fig. 2C-D). Remarkably, the stiffness gradient was steeper (*p<0.05; Figure 2−supplement table 1) for outer hair cells than for inner hair cells (Fig. 2E). As the characteristic frequency increased from 1 to 4 kHz, the hair-bundle stiffness K_{HB} increased by 240% from 2.5±0.2 mN/m (n = 19) to 8.6±0.5 mN/m (n = 21) for outer hair cells, but only by 120% from 1.7±0.2 mN/m (n = 19) to 3.8±0.4 mN/m (n = 19) for inner hair cells. At the 15-kHz position, where stiffness was only be recorded for inner hair cells (see Methods), $K_{HB} = 5.5 \pm 0.4$ mN/m (n = 14), thus still significantly lower (***p<0.001; Figure 2−supplement table 1) than in outer hair cells at the 4-kHz position. At each cochlear position, outer hair-cell bundles were stiffer than inner hair-cell bundles, with a stiffness ratio that increased from the apex to the base of the organ.

As also observed by others using fluid-jet stimulation of cochlear hair cells (Géléoc et al., 1997; Corns et al., 2014), we measured force-displacement relations that were remarkably linear (Fig. 2B and D), showing no sign of gating compliance (Howard and Hudspeth, 1988). There are at least two possible explanations for this observation. First, the rise time (~500 µs; Figure 2−figure supplement 3) of our fluid-jet stimuli may have been too long to outspeed fast adaptation, masking gating compliance (Kennedy et al., 2003; Tinevez et al., 2007). Second, gating forces –the change in tip-link tension evoked by gating of the transduction channels (Markin and Hudspeth, 1995)− may have been too weak to affect hair-bundle mechanics under our experimental conditions (Fettiplace, 2006; Beurg et al., 2008).

Parsing out the relative contributions of gating springs and stereociliary pivots to hair-bundle stiffness. There are two contributions to the stiffness of a hair bundle: $K_{HB} = K_{GS} + K_{SP}$. First, hair-bundle deflections modulate the extension of the gating springs that control the open probability of the mechano-electrical transduction channels; we denote by K_{GS} their contribution to hair-bundle stiffness. Second, bending of the actin core of the stereocilia at the stereociliary pivots, as well as stretching horizontal lateral links that interconnect the stereocilia, provides the remaining contribution K_{SP}. Because the gating springs are in series with the tip links, disrupting the tip links affords a means to estimate both K_{GS} and K_{SP}. We used local iontophoretic application of a Ca^{2+} chelator (EDTA; Methods and Fig. 1) to disengage the Ca^{2+}-dependent adhesion of the cadherin-related molecules forming each tip link (Kazmierczak et al., 2007). From the increased magnitude of the hair-bundle response to a given mechanical stimulus (see an example in Fig. 4A), we found that the gating springs contributed up to 50% of the total hair-bundle stiffness K_{HB}. Averaging over all inner and

outer hair cells that we tested, the relative contribution of the gating springs was $r = \mathrm{K_{GS}}/\mathrm{K_{HB}} = 22{\pm}2$ % (n = 71; Figure 3–figure supplement 1), where $1 - r$ is the amplitude ratio of hair-bundle movements before and after tip-link disruption. Both inner and outer hair cells displayed a gradient of gating-spring stiffness $\mathrm{K_{GS}} = r\,\mathrm{K_{HB}}$ (Fig. 3A). Between the 1-kHz and the 4-kHz positions, the gating-spring stiffness increased by 520% for outer hair cells but only by 300% for inner hair cells. Similarly, the contribution $\mathrm{K_{SP}} = (1 - r)\,\mathrm{K_{HB}}$ of the stereociliary pivots to hair-bundle stiffness displayed tonotopic gradients for both inner and outer hair cells (Fig. 3B).

Individual gating springs are stiffer in hair cells with higher characteristic frequencies. Both the pivot stiffness $\mathrm{K_{SP}}$ and the gating-spring stiffness $\mathrm{K_{GS}}$ are expected to vary according to hair-bundle morphology. Hair bundles get shorter and are composed of more numerous stereocilia as one progresses from the apex to the base of the cochlea (Figure 3–figure supplement 2), which ought to promote higher stiffness values. Are morphological gradients sufficient to explain the observed stiffness gradients of the hair bundle? Accounting for morphology, we write $\mathrm{K_{SP}} = \kappa\, N_{\mathrm{SP}}/\, h^2$ and $\mathrm{K_{GS}} = \mathrm{k_{GS}}\, N_{\mathrm{TL}}\gamma^2$, in which h, N_{SP}, N_{TL} correspond, respectively, to the height, the number of stereocilia and the number of (intact) tip links of the hair bundle, whereas $\gamma \propto 1/h$ is a geometrical projection factor (Figure 3–figure supplements 2-3). Remarkably, the intrinsic rotational stiffness κ of a single stereocilium in outer hair cells remained the same across the positions that we explored (Fig. 3C; Figure 3–supplement table 2). Similarly, with inner hair cells, there was no significant variation of the rotational stiffness between the 1- and 2-kHz locations as well as between the 4- and 15-kHz locations, although we observed an increase by 100% between the 2- and 4-kHz locations (Figure 3–supplement table 2). Averaging over the ensembles of outer and inner hair cells that we probed, the rotational stiffness $\kappa = 1.2{\pm}0.2$ fN·m/rad (n = 79) in outer hair cells was about 140% higher than the value $\kappa = 0.5{\pm}0.1$ fN·m/rad (n = 137) measured in inner hair cells. In contrast, the intrinsic stiffness k_{GS} of a single gating spring increased by 180% from 1.3±0.4 (n = 29) to 3.7±0.7 mN/m (n = 17) in outer hair cells and by 240% from 0.5±0.2 (n = 14) to 1.7±0.3 mN/m (n = 30) in inner hair cells, for characteristic frequencies that increased from 1 to 4 kHz and from 1 to 15 kHz, respectively (Fig. 3D). Thus, morphological gradients can account for the observed gradient in pivot stiffness $\mathrm{K_{SP}}$, but not for the observed gradient in gating-spring stiffness $\mathrm{K_{GS}}$ and in turn for the whole hair-bundle stiffness $\mathrm{K_{HB}}$. The hair-bundle morphology is not the sole determinant of hair-bundle mechanics.

Tip-link tension increases along the tonotopic axis. We then estimated the mechanical tension in the tip links at rest, *i.e.* in the absence of an external stimulus. The transduction channels close when the tip links are disrupted, indicating that the channels are inherently more stable in a closed state (Assad et al., 1991; Beurg et al., 2008; Indzhykulian et al., 2013). In functional hair bundles, tip-link tension is thought to bring the operating point of the transducer within the steep region of the sigmoidal relation between the channels' open probability and the position of the hair bundle, ensuring sensitive detection of hair-bundle deflections. If there is tension in the tip links, then disrupting these links must result in a positive offset in the resting position of the hair bundle (Assad et al., 1991; Jaramillo and Hudspeth, 1993).

In response to iontophoresis of a Ca^{2+} chelator (EDTA), we observed a net positive movement ΔX_{R} of the hair bundle at steady state, as expected if the tip links broke and released tension (Fig. 4A). Consistent with tip-link disruption, this movement was associated with a decrease in hair-bundle stiffness, as well as with closure of the transduction channels and loss of transduction (Fig. 4B). The positive offset in resting position upon tip-link disruption was observed at all positions that we explored along the tonotopic axis of the cochlea, both for inner and outer hair cells, demonstrating that the hair bundles were indeed under tension (Fig. 5A). In addition, we observed that the magnitude of the evoked movement increased significantly (**$p<0.01$; Figure 5–supplement table 1) from 9±3 nm (n = 13) to 45±10 nm (n = 12) for outer hair cells with characteristic frequencies that increased from 1 to 4 kHz. In contrast, we observed no significant difference among inner hair cells with characteristic frequencies that varied within the 1−15-kHz range ($p>0.05$; Figure 5–supplement table1): the positive offset was 21±2 nm (n = 71) over the whole ensemble of inner hair cells.

As a result, within the range of cochlear locations that we explored, we measured a steep gradient of hair-bundle tension for outer hair cells but a comparatively weaker gradient (*$p<0.05$; Figure 5–supplement table 1) for inner hair cells (Fig. 5B). Tension $T_{\mathrm{R}} = \mathrm{K}_{\mathrm{SP}}\,\Delta X_{\mathrm{R}}$ in the hair bundle was estimated as the product of the pivot stiffness K_{SP} and the positive offset ΔX_{R} in resting position evoked by tip-link disruption (Methods). The hair-bundle tension increased by nearly 13-fold from 18±7 pN (n = 15) to 248±59 pN (n = 17) for outer hair cells (characteristic frequencies: 1−4 kHz) but by only 3.3-fold from 24±5 pN (n = 33) to 100±22 pN (n = 12) for inner hair cells (characteristic frequencies: 1−15 kHz). Tension in the hair bundle resulted from the summed contributions of tension in individual tip links.

Dividing the tension T_{R} by the average number N_{TL} of intact tip links in our recordings and projecting the result along the oblique axis of the tip links (projection factor γ) provided estimates of the tension $t_{\mathrm{R}} = T_{\mathrm{R}}/(\gamma\, N_{\mathrm{TL}})$ in a single tip link. Remarkably, the observed gradients in hair-bundle tension (Fig. 5B) were not only due to an increase in the number of tip links that contributed to this tension (Figure 3−figure supplement 3), for tension in a single tip link also showed gradients (Fig. 5C). The single tip-link tension was comparable in the two types of cells at the 1-kHz location: 4.7±2.0 pN (n = 23) for outer hair cells and 5.9±1.3 pN (n = 43) for inner hair cells. However, at the 4-kHz location, the single tip-link tension had increased by 620% to 34±8 pN (n = 19) in outer hair cells but only by 170% to 16±4 pN (n = 17) in inner hair cells; at the 15-kHz location, tip-link tension in inner hair cells was 19±5 pN (n = 18). A linear regression of the relation between the single tip-link tension and the characteristic frequency confirmed that the gradient was significantly (*$p<0.05$; Figure 5−supplement table 1) steeper for outer hair cells.

Note that we have estimated here the stiffness and tension of a single tip-link complex along the hair bundle's axis of bilateral symmetry, which corresponds to the natural axis of mechanical stimulation in the cochlea. If the horizontal projection of tip links were actually oriented at an angle with respect to this axis, stiffness and tension ought to be larger along the tip-link axis than the values reported here. A systematic change in tip-link orientation along the tonotopic axis would also affect the gradients. These effects are expected to be small in inner hair cells, which are endowed with nearly linear hair bundles, but could be relevant for the V-shaped hair bundles of outer hair cells (Figure 3−figure supplement 2 and (Pickles et al., 1987)).

Tip-link tension first increases upon Ca^{2+} chelation. The dynamic response to an iontophoretic step of EDTA, and thus to a decrease of the extracellular Ca^{2+} concentration, was biphasic. The hair bundle first moved in the negative direction (arrowhead in Fig. 4A), before the directionality of the movement reverted and the bundle showed the positive movement associated with tip-link disruption. The negative movement was associated with an increased inward current of similar time course (Fig. 4B). Within the framework of the gating-spring model of mechanoelectrical transduction (Corey and Hudspeth, 1983; Markin and Hudspeth, 1995), this observation is readily explained if the evoked decrease in the extracellular Ca^{2+} concentration resulted in an increase in gating-spring tension, which both pulled the hair bundle in the negative direction and led to the opening of the transduction channels.

The magnitude of the negative movement at the peak showed no significant gradient and was similar between inner and outer hair cells, with an average magnitude of $\Delta X_{\mathrm{Ca}} = -26\pm2$ nm over the whole ensemble of hair cells (n = 83; Fig. 6A). However, because morphological gradients (Figure 3−figure supplement 2) resulted in gradients of pivot stiffness $\mathrm{K_{SP}}$ (Fig. 3B), the maximal increase $\Delta T = -\mathrm{K_{SP}}\,\Delta X_{\mathrm{Ca}}$ in hair-bundle tension was larger for hair cells with higher characteristic frequencies (Fig. 6B), as was the maximal tension t_{max} that a single tip link sustained before tip-link disruption (Fig. 6C). Going from 1-kHz to 4-kHz locations, this maximal tip-link tension displayed a gradient from 14±4 pN (n = 30) to 54±12 pN (n = 23) in outer hair cells and from 15±3 pN (n = 49) to 44±8 pN (n = 39) in inner hair cells; at the 15-kHz location, the maximal tension was not significantly different than at the 4-kHz location in inner hair cells.

When immersing the hair cells in low-Ca^{2+} saline, the negative movement was always followed by tip-link disruption and could thus not be observed twice with the same hair bundle. However, in six different preparations for which the hair bundle was immersed in saline with a higher Ca^{2+} concentration (500 µM) than usual (20 µM), we were able to preserve the integrity of the tip links and demonstrate that the negative movements could be reversible (Fig. 6D). Under such conditions, we observed that the absolute magnitude and the speed of the negative movement increased with the magnitude of the iontophoretic current. Notably, the hair bundle reached a new steady-state position when the iontophoretic step was long enough (Fig. 6E), suggesting that resting tension in the tip links could be modulated by the extracellular Ca^{2+} concentration, with higher tensions at lower Ca^{2+} concentrations.

DISCUSSION

Tonotopy of the mammalian cochlea is known to be associated with gradients of hair-bundle morphology (Wright, 1984; Lim, 1986; Roth and Bruns, 1992; Tilney et al., 1992), as well as of electrophysiological properties of the transduction apparatus (Ricci et al., 2003; Ricci et al., 2005; Fettiplace and Kim, 2014; Beurg et al., 2018). The work presented here reveals that tonotopy is also associated with gradients of intrinsic mechanical properties of the hair cell's tip-link complex. Specifically, by dissecting the relative contributions of the tip links and of the stereociliary pivots to the micromechanical properties of the hair bundle, we found that the gating springs that control the open probability of the mechanoelectrical transduction channels are stiffer (Fig. 3D) and subjected to higher mechanical tension (Fig. 5C) in hair cells that respond to higher characteristic frequencies. In return, our data raises the possibility of a

mechanical role of the tip-link complex in the process that sets the characteristic frequency of the hair cell.

The stiffness K_{HB} of the whole hair bundle displayed steeper gradients than those expected using the rough estimate $K_{HB} \propto N_{SP}/h^2$ from morphological changes (Figure 3–figure supplement 2) in length h and number of stereocilia N_{SP}. Computing the stiffness ratio between the most basal and the most apical cochlear location that we were able to probe, the measured stiffness ratios (Fig. 2E) were ~50% and ~70% larger than those expected from morphology for outer and inner hair cells, respectively. We interpret this result as the consequence of intrinsic gradients of the single gating-spring stiffness (Fig. 3D). Further emphasizing mechanical regulation at the level of the tip-link complex, we also observed that the rotational stiffness of a single stereocilium was nearly uniform across the cochlear locations that we tested, especially in outer hair cells (Fig. 3C). Stiffness gradients of hair bundles with disrupted tip links are thus entirely determined by morphology, in contradistinction to those observed with intact hair bundles.

Role of hair-bundle maturation in mechanical gradients. Our experiments were performed with hair cells from juvenile animals (P7-P10), before the onset of hearing. Hair-cell maturation progresses from base to apex in the cochlea (Wu and Kelley, 2012), which may thus have affected our estimates of mechanical gradients of the tip-link complex. However, because 92% percent of our recordings were performed at P8 or later (Methods), the tip-link complex ought to be nearly mature in our experiments, at least in outer hair cells (Roth and Bruns, 1992; Waguespack et al., 2007; Beurg et al., 2018). In inner hair cells, we cannot exclude that maturation of the hair-bundle morphology was still proceeding at the most apical cochlear positions explored in our study (Peng et al., 2009). Maturation sharpens the apex-to-base gradient of bundle length (Roth and Bruns, 1992); based on bundle morphology only, we would expect to underestimate stiffness gradients with immature inner hair cells.

Within the tip-link complex, transmembrane channel-like protein isoforms 1 and 2 (TMC1 and TMC2) are thought to be essential components of the transduction channels (Fettiplace and Kim, 2014; Pan et al., 2018). TMC2 is only transiently expressed after birth; TMC1 is expressed later than TMC2 but is fundamental to mechanoelectrical transduction of mature cochlear hair cells (Kawashima et al., 2011; Kim and Fettiplace, 2013). Stereociliary expression levels of TMC1, as well as their tonotopic gradients, were recently shown in mice to be nearly mature by P6, both in inner and outer hair cells, but TMC2 may still be present in apical inner hair cells until about P13 (Beurg et al., 2018). Because TMC2 confers larger

Ca^{2+} permeability to the transduction channels (Kim and Fettiplace, 2013), the Ca^{2+} influx at rest in the inner hair cells at P8-P10 may have been larger than at more mature developmental ages, possibly lowering tip-link tension (Fig. 6) and steepening its gradient.

How stiffness gradients may contribute to the tonotopic map. We observed that the hair-bundle stiffness increased by 240% over two octaves (1–4 kHz) of characteristic frequencies for outer hair cells and a similar increase but over 4 octaves (1–15 kHz) for inner hair cells (Fig. 2E). Whether or not stiffness would continue increasing along the same gradient towards more basal locations of the cochlea is unknown. If it were the case, we would expect a base-to-apex stiffness ratio of ~40 for outer hair cells, which is comparable to the base-to-apex ratio of characteristic frequencies in the rat cochlea (range: 0.5-50 kHz; (Viberg and Canlon, 2004)), but only of ~6 for inner hair cells. The interplay between the stiffness and mass of a hair bundle could in principle help specify the preferred frequency of vibration of the hair cell through passive mechanical resonance with sound stimuli (Frishkopf and DeRosier, 1983; Holton and Hudspeth, 1983; Manley et al., 1988; Freeman and Weiss, 1990; Gummer et al., 1996). The resonance frequency $\omega_{\mathrm{C}} = \sqrt{k/m}$ of a spring-mass system is given by the square root of the system's stiffness k divided by the mass m; it thus increases with stiffness, but relatively slowly. Assuming for simplicity that the bundle's mass remains nearly the same along the tonotopic axis (Tilney and Tilney, 1988), two orders of magnitude in frequency must be produced by a 10,000-fold increase in stiffness, corresponding to much steeper gradients than those reported here.

Alternatively, it has been proposed that the hair bundle could actively resonate with sound as the result of spontaneous oscillations (Martin et al., 2001; Hudspeth, 2008). Within this framework, the characteristic frequency is set by the frequency of the oscillator, which is expected to increase with the stiffness of the hair bundle (Vilfan and Duke, 2003; Tinevez et al., 2007; Martin, 2008; Barral et al., 2018). Notably, the relation may be steeper than that resulting from a passive spring-mass system, possibly approximating a linear dependence (Hudspeth et al., 2010). In this case, the stiffness gradient observed here (Fig. 2E) for outer hair cells, but not for inner hair cells, could be steep enough to be a major determinant of the tonotopic map.

Functional role of tension gradients. Tip-link tension is thought to control the open probability of the transduction channels, with higher tension promoting opening of the channels (Hudspeth and Gillespie, 1994). On this basis, a gradient of tip-link tension

(Fig. 5C) ought to result in a gradient of open probability. Yet, it has been shown in outer hair cells that the channels' open probability –the operating point of the transducer– remains remarkably uniform along the tonotopic axis, near a value of ½ (Johnson et al., 2011). To explain this observation, we note that the tension gradient for outer hair cells is associated with a gradient of single-channel conductance (Beurg et al., 2006; Beurg et al., 2015; Beurg et al., 2018). As a consequence, the magnitude of the Ca^{2+} influx into transducing stereocilia is expected to increase with the characteristic frequency of the hair cell. Manipulations that affect the extracellular or the intracellular Ca^{2+} concentration indicate that the transduction channels close at increased Ca^{2+} concentrations (reviewed in (Fettiplace and Kim, 2014)), possibly because the channels are harder to open when the Ca^{2+} concentration is higher near the channel's pore (Cheung and Corey, 2006). Thus, the gradient of tip-link tension reported here (Fig. 5C) may compensate for the effects of the conductance gradient on the open probability: channels with higher conductance impart higher Ca^{2+} influxes (closing the channels) but are also subjected to higher tension (opening the channels), perhaps maintaining an optimal operating point for the transducer at all cochlear locations.

Tension in the tip links is thought to be produced actively by pulling forces from molecular motors interacting with the actin core of the stereocilia at the upper insertion point of the tip link (Gillespie and Muller, 2009). The observed tension gradient in turn implies that, towards basal cochlear locations, there are more motors or that each motor exerts higher forces than near the apex. Notably, the tip links of inner-hair-cell bundles were found to bear less tension than those of outer hair cell (Fig. 5B-C). This property qualitatively makes sense, for the open probability of the transduction channels is thought to be smaller in inner hair cells than in outer hair cells (Russell and Sellick, 1983). There is also no, or only a weak, gradient of the single-channel conductance in inner hair cells (Beurg et al., 2006; Beurg et al., 2018), which parallels the relatively weak gradient of tip-link tension observed here.

Tip-link tension may be high enough to alter tip-link conformation and affect gating-spring stiffness. The tip link is composed of the association of two cadherin-related proteins, cadherin-23 and protocadherin-15 (PCDH15) (Kazmierczak et al., 2007). Molecular dynamics simulations have suggested that a bend between extracellular cadherin (EC) repeats 9 and 10 of PCDH15 may confer some compliance to otherwise rigid tip links (Araya-Secchi et al., 2016). Tensions higher than ~10 pN are predicted to evoke complete unbending of EC9-10, resulting in significant stiffening of the tip link. Assuming that PCDH15 in the tip link forms a dimer (Kazmierczak et al., 2007; Ge et al., 2018) and that tip-link tension is

equally shared by the two filaments, our estimates of tip-link tension (Fig. 5C) are compatible with a contribution of the bending elasticity of EC9-10 to gating-spring stiffness at the apex of the rat cochlea, especially in inner hair cells. In outer hair cells, as one progresses from the very apex towards more basal cochlear locations, tension may quickly become too high to allow a bent conformation in EC9-10. At the 4-kHz location, we estimated a resting tip-link tension of ~35 pN. Taking the measured unfolding forces of Ig domains in titin as a reference (Rief et al., 1997), tip-link tension might actually be high enough to evoke unfolding of EC domains, at least under resting conditions or at physiological loading rates. Recent evidence suggests that unfolding a various number of EC domains may contribute to a gradation of gating-spring stiffness (Bartsch et al., 2018; Bartsch and Hudspeth, 2018).

Notably, the estimated gradients of gating-spring tension (Fig. 5C) were associated with gradients of gating-spring stiffness (Fig. 3D): stiffer gating springs are subjected to more resting tension. Strain stiffening is a common phenomenon associated with the entropic elasticity of macromolecules, including the tip-link component PCDH15 (Bartsch et al., 2018), as well as with filamentous protein networks (Bustamante et al., 1994; Rief et al., 1997; Kang et al., 2009). A tension gradient may thus in part explain the existence of the observed gradient of gating-spring stiffness. Alternatively, the gating-spring stiffness could vary if the gating spring were composed of a variable number of compliant molecules operating in parallel and connected to a single tip link.

Tip-link tension depends on calcium. Upon iontophoretic application of a Ca^{2+} chelator (EDTA), before tip-link disruption, we observed that the hair bundle first moved in the negative direction and that this movement was associated with a concomitant opening of the transduction channels (Fig. 4). Calcium acts as a permeant channel blocker of the transduction channels (Fettiplace and Kim, 2014). Lowering the extracellular Ca^{2+} concentration is thus expected to increase the magnitude of the current flowing through open transduction channels but not to produce hair-bundle movements, at least as the result of block release only. A decrease of the extracellular Ca^{2+} concentration also promotes opening of the transduction channels (Hacohen et al., 1989; Johnson et al., 2011). Within the framework of the gating-spring model of mechanoelectrical transduction, channel opening must reduce gating-spring extension and in turn tension, fostering *positive* movements of the hair bundle. Thus, the observed *negative* movements cannot result from internal forces associated with channel gating. Instead, our observations are readily explained if the evoked reduction of extracellular Ca^{2+} concentration resulted in an increase of tip-link (and thus

gating-spring) tension. If tip-link tension at rest is set by myosin molecular motors that pull on the tip links (Hudspeth and Gillespie, 1994), then the motor force must increase at decreased Ca^{2+} concentrations.

Alternatively, a negative deflection would also be produced if lowering the extracellular Ca^{2+} concentration evoked stiffening (Martin et al., 2003; Beurg et al., 2008) or shortening of the gating springs, increasing tension in the tip links. However, this mechanism would result in a negative steady-state offset of the bundle's resting position (Fig. 6E) only if there were no or little myosin-based adaptation –usually called 'slow adaptation'(Hudspeth and Gillespie, 1994; Peng et al., 2013)– to relax the tension change and return the hair bundle near its initial resting position. Because we observed the mechanical correlate of slow adaptation in response to force steps (Figure 2−figure supplement 5), a Ca^{2+}-dependent regulation of tip-link tension via a change of gating-spring stiffness or length appears unlikely. This inference may be relevant to recent data implicating the stereociliary membrane as a key regulator of transduction-channel gating. Calcium ions have indeed been proposed to interact extracellularly with the local lipid environment of the transduction channels, promoting lower values of the channels' open probability (Peng et al., 2016). Our recordings (Fig. 4B and Fig. 6D-E) are consistent with this hypothesis but a change in membrane mechanics wouldn't explain the observed steady-state increase in tip-link tension (Fig. 6E) if slow adaptation happens in these cells (Figure2− figure supplement 5).

Interestingly, depolarization of rat outer hair cells was previously shown to evoke positive movements of the hair bundle (Kennedy et al., 2006). Both depolarization and chelation of extracellular Ca^{2+} are expected to reduce the intracellular Ca^{2+} concentration in the vicinity of the transduction channel's pore. Yet, the directionality of active hair-bundle movements is opposite in the two studies, suggesting that the hair bundle can operate in two regimes (Tinevez et al., 2007). In the first regime (Kennedy et al., 2006), the response to Ca^{2+} changes is dominated by gating forces (Howard and Hudspeth, 1988) so that the resting tension in the tip links is nearly the same before and after application of the stimulus. In the other regime (our study), Ca^{2+}-evoked changes of the resting tension in the tip links (Fig. 6) dominate gating forces. In the chicken cochlea, depolarization of the hair cell was reported to evoke negative movements of the hair bundle (Beurg et al., 2013), a directionality in agreement with that found here (Fig. 4A). In addition, it has been shown in the bullfrog's sacculus (Tinevez et al., 2007) and the turtle's cochlea (Ricci et al., 2002) that the response of different hair cells to a given Ca^{2+} change can be of either directionality and that the directionality of the response for a given hair cell can even be reversed by applying a position offset to the hair

bundle. The two regimes of active hair-bundle motility can thus potentially coexist within the same hair cell, but only if gating forces are strong enough (Tinevez et al., 2007). We measured force-displacement relations that were remarkably linear (Fig. 2B and D), showing no sign of gating compliance (Howard and Hudspeth, 1988). This observation confirms that gating forces were relatively weak under our experimental conditions, although others have shown that gating compliance can be measured with mammalian cochlear hair cells (Russell et al., 1992; Kennedy et al., 2005).

Mechanical gradients reflect the division of labor between inner and outer hair cells. Stiffness (Fig. 2E) and tension (Fig. 5B) gradients were steeper for outer hair cells, which serve primarily as mechanical amplifiers of sound-evoked vibrations, than for inner hair cells, the true sensors of the inner ear (Hudspeth, 2014). Other properties, such as the height of the hair bundle (Wright, 1984; Lim, 1986; Roth and Bruns, 1992) or the conductance of the transduction channels (Beurg et al., 2006; Beurg et al., 2018), show a similar behavior. Thus, the division of labor between inner and outer hair cells may impart more stringent regulatory constrains to outer hair cells to tune their mechanoreceptive antenna according to the local characteristic frequency of the cochlear partition. However, the exact contribution of the hair bundle to frequency tuning remains unsure and, more generally, the mechanism that specifies the characteristic frequency remains a fundamental problem in auditory physiology. This may be in part because frequency selectivity cannot be ascribed to one element only, for instance the passive resonant property of the basilar membrane that was characterized in the pioneering work of von Bekesy (Von Békésy and Wever, 1960). Various models of cochlear mechanics instead indicate that the characteristic frequency emerges from an active dynamic interplay between somatic electromotility of outer hair cells (Ashmore, 2008) and the micromechanical environment, including the basilar and tectorial membranes ,as well as the hair bundle (Nobili and Mammano, 1996; Hudspeth et al., 2010; Ó Maoiléidigh and Jülicher, 2010; Meaud and Grosh, 2011; Hudspeth, 2014; Reichenbach and Hudspeth, 2014). Mechanical tuning of the inner constituents of the cochlear partition appears to happen at many scales: from the mesoscopic scale of the basilar and tectorial membranes, to the cellular scale of the hair bundle and hair-cell soma, down to the molecular scale of the hair cell's transduction apparatus. Our work demonstrates that tonotopy is associated, in addition to other factors, with stiffness and tension gradients of the tip-link complex.

METHODS

Experimental preparation. All experimental procedures were approved by the Ethics committee on animal experimentation of the Institut Curie; they complied with the European and French-National Regulation for the Protection of Vertebrate Animals used for Experimental and other Scientific Purposes (Directive 2010/63; French Decree 2013-118). Experiments were performed on excised cochlear coils of Sprague Dawley rats (Janvier Labs) between postnatal day 7 and 10 (P7–P10), with 8% of the cells at P7, 75% at P8–P9 and 17% at P10. The dissection of the cochlea followed a published procedure (Kennedy et al., 2003). In short, we cracked open the bony shell covering the cochlear tissue, unwound the cochlear tube from the modiolus, removed the stria vascularis, and gently peeled the tectorial membrane. Apical or middle turns of the organ of Corti were positioned under strands of nylon fibres in the experimental chamber. We recorded from inner hair cells at 4 positions along the longitudinal axis of the cochlea (Fig. 1A), corresponding to fractional distances of 5%, 10%, 20%, and 50% from the cochlear apex. According to the tonotopic map in this species (Viberg and Canlon, 2004), these cells were tuned at characteristic frequencies of 1, 2, 4, and 15 kHz, respectively. We also recorded from outer hair cells but only at the first three positions along the tonotopic axis. We have attempted to record from outer hair cells farther towards the cochlear base, in particular at the 7 kHz location. However, our success rate was too low to get reliable estimates of tip-link tension and gating-spring stiffness, the primary goal of our work. Among possible reasons, basal outer hair cells might not withstand immersion in low-Ca^{2+} (~20 µM) saline, a condition that we used to disrupt the tip links. In addition, the hair bundles of outer hair cells are smaller towards the base; monitoring their movements from direct imaging on photodiodes (see 'Microscopic apparatus' below) thus gets harder because the contrast of the image is lower.

The tissue was bathed in a standard saline containing 150 mM NaCl, 6 mM KCl, 1.5 mM $CaCl_2$, 2 mM Na-pyruvate, 8 mM glucose and 10 mM Na-HEPES. In some experiments, we used a low-Ca^{2+} saline containing 150 mM NaCl, 6 mM KCl, 3.3 mM $CaCl_2$, 4 mM HEDTA, 2 mM Na-pyruvate, 8 mM glucose, and 10 mM Na-HEPES. As measured with a Ca^{2+}-sensitive electrode, this solution had a free Ca^{2+} concentration of 22 µM, similar to that found in rat endolymph (Bosher and Warren, 1978). All solutions had a pH of 7.4 and an osmotic strength of 315 $mOsm \cdot kg^{-1}$. Experiments were performed at a room temperature of 20–25°C.

Microscopic Apparatus. The preparation was viewed through a ×60 water-immersion objective of an upright microscope (BX51WI, Olympus). The tips of individual hair bundles

were imaged at a magnification of ×1,000 onto a displacement monitor that included a dual photodiode. Calibration was performed before each recording by measuring the output voltages of the monitor in response to a series of offset displacements of the photodiode. For hair-bundle movements that did not exceed ±150 nm in the sample plane, the displacement monitor was linear.

Iontophoresis of a Ca^{2+} Chelator. We used iontophoresis to apply the calcium chelator EDTA in the vicinity of a hair bundle (Fig. 1B) and disrupt its tip links (Assad et al., 1991; Jaramillo and Hudspeth, 1993; Marquis and Hudspeth, 1997). Coarse microelectrodes were fabricated from borosilicate capillaries with a pipette puller (P97, Sutter Instrument); their resistance was 1 MΩ when filled with 3 M KCl and immersed in the same solution. In experiments, the electrodes were filled with a solution containing 100 mM EDTA and 25 mM KCl. The electrode's tip was positioned at ~3 μm from the hair bundle. A holding current of +10 nA was continuously applied to counteract the diffusive release of EDTA from the electrode. The stimulus consisted of a –100-nA current step on top of the holding current, resulting in a net iontophoretic current of –90 nA. To facilitate tip-link disruption upon EDTA iontophoresis, the cochlear tissues were immersed in low-Ca^{2+} saline (~20-μM Ca^{2+}).

Mechanical stimulation and stiffness measurements. The hair bundles of inner and outer hair cells were mechanically stimulated using a fluid-jet device (Kros et al., 1992; Géléoc et al., 1997; Johnson et al., 2011). Pipettes were pulled from borosilicate glass (TW150-F, World Precision Instruments); their tip diameter was adjusted within a range of 5–10 μm. Fluid flow through a pipette was driven by a voltage command to a piezoelectric disk (Murata 7BB-27-4). Any steady-state flow coming in or out of the pipette was nulled by changing the hydrodynamic pressure inside the fluid-jet pipette; the hydrodynamic pressure was adjusted with a syringe connected to the body of the fluid-jet device. The fluid-jet pipette was positioned on the abneural side of the bundle along the hair bundle's axis of mirror symmetry (Fig. 1C). Fluid coming out the pipette thus deflected the hair bundles towards the shortest stereociliary row, closing the ion channels that mediate mechanoelectrical transduction. This direction of bundle movement is defined as the negative direction in this paper; conversely, positive movements were directed towards the tallest row of stereocilia, fostering opening of the transduction channels. Mechanical stimuli were applied as 100-ms paired-pulse steps (Fig. 2 and Figure 2–figure supplement 3), or 60-Hz sinusoids (Fig. 4) with the magnitude of driving voltages varying between 0 and 60 V.

For stiffness measurements, we measured hair-bundle movements evoked by 100-ms force steps (Fig. 2; see the force-calibration procedure below). The bundle displacement was measured 5–10 ms after the onset of the step stimulus; the stiffness was given by the slope of the relation between the force (noted F in the following) and the displacement of the bundle's tip. These measurements were performed in standard saline.

Applying and measuring forces with the fluid jet. We describe here how we calibrated the hydrodynamic drag force F_D applied to the hair bundle by a fluid jet by using a flexible glass fiber of known stiffness as a reference. The method is based on a published procedure (Géléoc et al., 1997) that we refined to account for the non-uniform velocity field of the fluid (Figure 2–figure supplement 1). Using a generalized Stokes equation (Leith, 1987), the drag force can be written as $F_D = 6\pi\eta R_{\mathrm{HB}}\, U$, in which η is the viscosity of the surrounding fluid and R_{HB} is the effective hydrodynamic radius of the bundle. The effective radius R_{HB} was approximated by that of a prolate ellipsoid of short axis h and long axis W, which correspond to the bundle's height and width, respectively. For a fluid flow perpendicular to the axis of rotational symmetry of the ellipsoid, this yields:

$$R_{\mathrm{HB}} \cong 4h\Big/\left\{3\left[\phi/(\phi^2-1) + \left((2\phi^2-3)\ln\left(\phi+\sqrt{\phi^2-1}\right)\right)\Big/(\phi^2-1)^{3/2}\right]\right\}, \quad (1)$$

in which $\phi = W/h$ represents the aspect ratio of the ellipsoid (Happel and Brenner, 2012). We note that the hydrodynamic radius given by Equation 1 is exact only for an ellipsoid immersed in an infinite volume of fluid, whereas the hair bundle instead stands erect at the apical surface of the hair cell; this expression is thus an approximation. Figure 3–supplement table 1 and Figure 3–figure supplement 2 recapitulate the values of parameters h and W that we used to model inner and outer hair-cell bundles along the tonotopic axis of the rat cochlea, as well as the resulting values of R_{HB}. The effective velocity $U \cong \int_{-W/2}^{W/2} v_X(x,y)\, dy/W$ was estimated by computing the mean of the velocity field $v_X(x,y)$ of the fluid over the width W of the hair bundle. Here, $v_X(x,y) = \vec{v}\cdot\vec{e}_X$ is the projection of the fluid velocity $\vec{v}$ on the axis of mechanosensitivity (axis X) of the hair bundle; its value is estimated along the axis (Y) perpendicular to axis X for a bundle positioned at a distance x from the mouth of the fluid-jet pipette (Figure 2–figure supplement 1A). Using bead tracers, we found that the velocity profile $v_X(x,y)$ obeyed (Schlichting, 1933)

$$v_X(x,y) = V_{\max}(x)/(1+(y/A(x))^2)^2, \quad (2)$$

where $V_{\max}(x)$ and $A(x)$ characterize, respectively, the maximal speed and the lateral extension of the velocity field at position x (Figure 2−Figure supplement 1B-D). By integrating the velocity profile, we obtain an expression for the force

$$F_D = 6\pi\eta R_{\mathrm{HB}}\, \beta_{\mathrm{HB}}\, V_{\max}\,, \tag{3}$$

where $\beta_{\mathrm{HB}} = \beta(w) = \frac{1}{2w}(w/(1+w^2) + \tan^{-1} w)$ is a constant that depends on the normalized width of the hair bundle $w = W/(2A)$. Thus, calibrating the force F_D is equivalent to calibrating the maximal fluid velocity $V_{\max}$.

To estimate $V_{\max}$, we measured the force $\bar{F}_D \cong 6\pi\eta R_{\mathrm{F}}\, \bar{U}$ applied by the same jet on a calibrated glass fiber, whose longitudinal axis was oriented perpendicularly to that of the fluid-jet pipette. Given the diameter D_{F} of the fiber, the effective hydrodynamic radius of a cylindrical fiber was calculated as $R_{\mathrm{F}} = 2L/[3(\ln(L/D_{\mathrm{F}}) + 0.84)]$ (Tirado and Torre, 1979). Because the conical fluid jet intersected the fiber over a length $L > W$, the effective fluid velocity $\bar{U} \cong \int_{-L/2}^{+L/2} v_X(x,y)\, dy/L = \beta_{\mathrm{F}}\, V_{\max}$ for the fiber was smaller than the effective velocity U for the hair bundle, where $\beta_{\mathrm{F}} = \beta(L/(2A)) < \beta_{\mathrm{HB}}$. In practice, we used $L(x) = 2\,x\,\tan\alpha + D_{\mathrm{FJ}}$, where α is the half-aperture of the conical fluid jet that was visualized using a dye (Coomassie Brilliant Blue; Figure 2−figure supplement 2) and D_{FJ} is the diameter of the mouth of the fluid-jet pipette. We noticed that $L(x) \cong 2A(x)$ (Figure 2–figure supplement 1; figure supplement 2). We used this property to estimate $\beta_{\mathrm{HB}} \cong \beta(W/L)$ and $\beta_{\mathrm{F}} \cong \beta(1)$ without having to measure A directly in every experiment.

In experiments, the projected horizontal distance between the tip of the fluid-jet pipette and the hair bundle or the fiber was fixed at $x \cong 8$ µm (mean ± SD: 7.8±0.6 µm; range: 5.9–8.8 µm). Flexible fibers of diameters $D_{\mathrm{F}} =$ 0.7–1.5 µm and stiffness $k_{\mathrm{F}} = 0.2$–2 mN/m were fabricated and calibrated as described before (Bormuth et al., 2014); their effective hydrodynamic radii varied within a range of $R_{\mathrm{F}} = 2.5$–3.2 µm. A fluid jet of given magnitude elicited a force $\bar{F}_D = k_{\mathrm{F}}\, \Delta X$, where ΔX is the measured deflection of the fiber. The relation between the force $\bar{F}$ applied to a fiber and the voltage command to the fluid-jet device was linear; its slope provided the calibration constant C (Figure 2−figure supplement 3). When stimulating a hair bundle, a voltage command V_C to the fluid-jet device thus elicited a force $F_D \cong GCV_C$, where $G = F_D/\bar{F}_D = (\beta_{\mathrm{HB}} R_{\mathrm{HB}})/(\beta_{\mathrm{F}} R_{\mathrm{F}})$. We used G =1.4±0.1 (mean ± SD; range: 1.27−1.65) for inner hair cells and G =1.3±0.1 (mean ± SD; range: 1.12−1.47) for outer hair cells. Thus, we estimate that the force applied on the hair bundle was 30−40% higher than that measured on the calibration fiber using the same jet of fluid. In practice,

we calculated G in each experiment from the geometrical parameters of the fluid-jet pipette, the calibration fiber, and the hair bundle. We noticed that $L(x) \cong 2A(x)$; at a distance $y = L/2$ from the center of the fluid jet ($y = 0$), the fluid velocity is expected to be 25% of the maximal value. Thus, some of the moving fluid was not taken into account in our estimates of the force acting on the fiber, resulting in an underestimation. However, taking $L(x) = 4A(x)$ resulted in an increase of G by only 5% while the fluid velocity dropped to 4% of the maximal value at the edge of the fluid cone (in $y = L/2 = 2A$).

All the forces reported in this work correspond to the effective force F that one would have to apply at the bundle's tip to evoke the same bundle deflection X as the hydrodynamic drag force F_D actually exerted by the fluid jet and distributed over the height of the hair bundle. Correspondingly, the stiffness of the hair bundle was calculated as the slope of the force-displacement relation $F(X)$. In the following, we develop an approximate description of hair-bundle mechanics to relate the effective force F to the drag force F_D. Modelling the hair bundle as a pivoting solid (Kozlov et al., 2007; Kozlov et al., 2011), we write the torque produced by the fluid jet as $\Gamma = \int_0^h f(z)\, z\, dz = \kappa_{HB}\, \theta$. Here, h is the height of the hair bundle, f is the drag force per unit (vertical) length experienced by the hair bundle at a vertical distance z from the apical surface of the hair cell, κ_{HB} is the rotational stiffness of the hair bundle, and $\theta \cong X/h$ is the pivoting angle corresponding to the deflection X measured at the bundle's top. With these notations, the total drag force on the hair bundle reads $F_D = \int_0^h f(z)\, dz$. Assuming that the drag force per unit length $f \propto v(z)$ is proportional to the local fluid velocity $v(z)$ and that the condition of no-slip at the apical surface of the hair cell ($v(z = 0) = 0$) imposes a linear velocity profile $v(z) = v(h)\, z/h$, we take $f \propto z$. Injecting this expression into the integrals defining the torque Γ and the total drag force F_D, we find $\Gamma = \frac{2}{3} F_D h$. As a result, we identify the effective force $F = \frac{2}{3} F_D$ that must be applied at the bundle's top to evoke the same torque as the fluid jet; the effective force F is smaller than the total drag force F_D exerted by the fluid jet, corresponding to a ratio $F/F_D = 2/3$.

To test our force-calibration procedure for the fluid jet, we performed a control experiment using hair-cell bundles from the sacculus of the frog (strain "Rivan92" of *Rana ridibunda* (Neveu, 2009)). Details of the experimental preparation have been published elsewhere (Tinevez et al., 2007). In a similar preparation, the hair bundles have been shown to be very cohesive (Kozlov et al., 2007). As a result, the stereocilia are constrained to move as a unit in response to point-force application at the kinociliary bulb with a flexible fiber, allowing for

well-controlled stiffness measurements (Martin et al., 2000; Bormuth et al., 2014). We compared stiffness estimates from stimulation with fluid jets and flexible fibers (Figure 2–figure supplement 4). From a sample of 13 hair bundles, we found a stiffness of 0.40±0.17 mN/m (mean±SD) using fluid-jet stimulation and of 0.42±0.16 mN/m (mean±SD) using fiber stimulation; the mean values of the stiffness estimates were not statistically different (paired-sample t-test; ***$p<0.001$). The good agreement between the two methods gave us confidence that the procedure that we used to calibrate the fluid jet is satisfactory.

Electrophysiological recordings. We used the patch-clamp technique to measure mechano-electrical transduction currents. Borosilicate patch pipettes were filled with an intracellular solution containing 142 mM CsCl, 3.5 mM $MgCl_2$, 1 mM EGTA, 5 mM Na_2-ATP, 0.5 mM Na_2-GTP and 10 mM HEPES (pH=7.3, 295 mOsmol/kg). When immersed in standard saline, these pipettes had a resistance of 1.5–3 MΩ. A patch pipette was inserted in the organ of Corti through a pre-formed hole in the reticular lamina and approached parallel to the hair cell rows towards the soma of a target hair cell. During the approach, standard saline was abundantly perfused to protect the Ca^{2+}-sensitive tip-links from EGTA. Hair cells were whole-cell voltage clamped at a holding potential of −80 mV; transduction currents were low-pass filtered at 1-10 kHz (Axopatch 200B; Axon Instruments). No correction was made for the liquid-junction potential. The series resistance was always below 10 MΩ and was compensated up to 70%. To disrupt the tip links with EDTA iontophoresis, the solution bathing the cells was changed to low-Ca^{2+} saline after the cell was patched; the solution change was performed either with a perfusion or with a Picospritzer (Picospritzer III, Parker).

Scanning electron microscopy. Cochleae from P8 rats were processed with osmium tetroxide/thiocarbohydrazide, as previously described (Furness et al., 2008). Samples were analysed by field emission scanning electron microscopy operated at 5 kV (Jeol JSM6700F). The number of stereocilia in inner and outer hair-cell bundles was estimated from electron micrographs at each of the cochlear locations where we performed mechanical and electrophysiological measurements (Figure 3–figure supplement 2; Figure 3−supplement table 1).

Estimating the number of intact tip links in a hair bundle. We performed patch-clamp recordings of the transduction current I_{MAX} elicited at saturation by large hair-bundle deflections (Figure 3–supplement figure 3). In inner hair cells, the number of intact tip links $N_{\mathrm{TL}} = I_{\mathrm{MAX}}/I_1$ was calculated by dividing the saturated current I_{MAX} for the whole hair bundle by the published estimate $I_1 = 35.4$ pA for the transduction current flowing through

the tip of a single transducing stereocilium (Beurg et al., 2009); electron microscopy has indeed shown that there is precisely one tip link per stereocilium in an intact hair bundle (Pickles et al., 1984; Kachar et al., 2000). We used the same value of I_1 at all cochlear locations (Beurg et al., 2006; Beurg et al., 2018). Given the magnitude $i = 15$ pA of the current flowing through a single transduction channel, there was on average $I_1/i = 2.36$ transduction channels per transducing stereocilium (Beurg et al., 2006). In outer hair cells, there is no direct estimate of I_1. However, the unitary current i was shown to increase (Beurg et al., 2006; Beurg et al., 2015; Beurg et al., 2018) from 8.3 pA to 12.1 pA when the hair cell's characteristic frequency increases from 4 kHz to 14 kHz (Beurg et al., 2006). All these currents were measured under the same experimental conditions as ours, in particular using a −80 mV holding potential and with the hair cells immersed in a standard saline containing 1.5 mM Ca^{2+}. Assuming a linear relation between the unitary current and the position of the hair cell along the tonotopic axis of the cochlea (Beurg et al., 2015; Beurg et al., 2018), we inferred the unitary currents at other cochlear locations. We then assumed that the average number of transduction channels per tip link was 2.36, as estimated in inner hair cells (Beurg et al., 2009). The number of intact tip links was then calculated as $I_{\mathrm{MAX}}/(2.36\, i)$. We performed this measurement for 10 hair cells at each cochlear location, both for inner and outer hair cells, to calculate the average number of intact tip links in any given hair cell. In these experiments, the hair cells were immersed in standard saline.

Recent measurements in the mouse cochlea have revealed that unitary currents may represent an ensemble average over multiple conductance states, raising the possibility that these currents are produced by a few (up to 5) identical transduction channels that gate cooperatively (Beurg et al., 2018). This finding does not affect our estimates, because the current that flows through a single stereocilium stays the same, whether or not it results from cooperative gating of multiple channels or from gating of an effective channel endowed with the same conductance as the total conductance of the group.

Signal Generation and Acquisition. All signals were generated and acquired under the control of a computer running a user interface programmed with LabVIEW software (version 2011, National Instruments). Command signals were produced by a 16-bit interface card at a sampling rate of 25 kHz (PCI-6733, National Instruments). A second interface card (PCI-6250, National Instruments) conducted signal acquisition with a precision of 16 bits. Sampling rates for signal generation and acquisition varied within the range 2.5−25 kHz. All

signals were conditioned with an eight-pole Bessel antialiasing filter adjusted to a low-pass half-power frequency at half the sampling rate of signal acquisition.

Statistical significance. Unless otherwise noted, all results are quoted as mean ± standard error of the mean (*n*) with a number *n* of cells of at least 10 per group. G-Power analysis ensured that this number was sufficient to achieve a signal-to-noise ratio of 1–1.5, with 80% power at a 5% significance level. We performed a one-way ANOVA to assay statistical significance of the measured mean-value variation of a given property, *e.g.* the hair-bundle stiffness, between the different cochlear locations for inner (IHC) or outer (OHC) hair cells. We also used two-tailed unpaired Student's *t*-tests with Welch's correction when comparing mean values between two groups of a given hair-cell type (IHC or OHC) with different characteristic frequencies or between the two cell types (IHC/OHC) with a given characteristic frequency. Stars correspond to p-values with *p < 0.05, **p < 0.01, and ***p < 0.001, whereas 'n.s.' (p > 0.05) indicates non-significant differences. To determine whether variables estimated from the product of M independent variables X_i ($i = 1 \,..\, M$) had means that were statistically different, we first calculated the standard error of the mean $\sigma_{\prod X_i}$of the product and the effective number of degrees of freedom ν_{eff} of the product. Defining $\overline{X}_\iota$ as the mean value of the variable X_i over n_i measurements, s_i the standard deviation and $\sigma_i = s_i/\sqrt{n_i}$ the standard error of the mean, the standard error of the mean for the product was calculated as $\sigma_{\prod X_i} = \prod \overline{X}_\iota \sqrt{\sum \left(\frac{\sigma_i}{\overline{X}_\iota}\right)^2}$ and the effective number of degrees of freedom associated with the product was calculated using the Welch-Satterthwaite approximation as $\nu_{\mathrm{eff}} = \left[\sigma_{\prod X_i}/\prod \overline{X}_\iota\right]^4 / \sum \frac{1}{n_i - 1}\left(\frac{\sigma_i}{\overline{X}_\iota}\right)^4$. Finally, we characterized tonotopic gradients by performing weighted linear regressions, in which the weight applied to each data point was given by the inverse of the squared standard error of the mean. We then applied a *t*-test on the resulting coefficients to determine whether the observed difference between the gradients measured with inner and outer hair cells was statistically significant. The results of all statistical analyses are listed in supplement tables associated to the main figures.

Acknowledgements:

We thank Benoît Lemaire and Rémy Fert from the machine shop of the Curie Institute, Prof. Walter Marcotti for help in the design of our fluid-jet device, Jérémie Barral for a critical reading of the manuscript and Christine Petit for fruitful discussions. This research was supported by the French National Agency for Research (ANR-11-BSV5 0011 and ANR-16-CE13-0015) and by the Labex Celtisphybio ANR-10-LABX-0038 part of the Idex PSL. M.T. is alumnus of the Frontiers in Life Science PhD program of Université Paris Diderot and thanks the Fondation Agir pour l'Audition for a doctoral fellowship.

REFERENCES

Araya-Secchi R, Neel BL, Sotomayor M (2016) An elastic element in the protocadherin-15 tip link of the inner ear. Nature communications 7:13458.

Ashmore J (2008) Cochlear outer hair cell motility. Physiol Rev 88:173-210.

Assad JA, Shepherd GM, Corey DP (1991) Tip-link integrity and mechanical transduction in vertebrate hair cells. Neuron 7:985-994.

Barral J, Jülicher F, Martin P (2018) Friction from Transduction Channels' Gating Affects Spontaneous Hair-Bundle Oscillations. Biophysical journal 114:425-436.

Bartsch TF, Hudspeth A (2018) A New Twist on Tip Links. Neuron 99:423-425.

Bartsch TF, Hengel FE, Oswald A, Dionne G, Chipendo IV, Mangat SS, El Shatanofy M, Shapiro L, Mueller U, Hudspeth AJ (2018) The elasticity of individual protocadherin 15 molecules implicates cadherins as the gating springs for hearing. bioRxiv:503029.

Beurg M, Tan X, Fettiplace R (2013) A prestin motor in chicken auditory hair cells: active force generation in a nonmammalian species. Neuron 79:69-81.

Beurg M, Evans MG, Hackney CM, Fettiplace R (2006) A large-conductance calcium-selective mechanotransducer channel in mammalian cochlear hair cells. J Neurosci 26:10992-11000.

Beurg M, Nam JH, Crawford A, Fettiplace R (2008) The actions of calcium on hair bundle mechanics in mammalian cochlear hair cells. Biophys J 94:2639-2653.

Beurg M, Fettiplace R, Nam JH, Ricci AJ (2009) Localization of inner hair cell mechanotransducer channels using high-speed calcium imaging. Nat Neurosci 12:553-558.

Beurg M, Xiong W, Zhao B, Muller U, Fettiplace R (2015) Subunit determination of the conductance of hair-cell mechanotransducer channels. Proc Natl Acad Sci U S A 112:1589-1594.

Beurg M, Cui R, Goldring AC, Ebrahim S, Fettiplace R, Kachar B (2018) Variable number of TMC1-dependent mechanotransducer channels underlie tonotopic conductance gradients in the cochlea. Nat Commun 9:2185.

Bormuth V, Barral J, Joanny J-F, Juelicher F, Martin P (2014) Transduction channels' gating can control friction on vibrating hair-cell bundles in the ear. Proc Natl Acad Sci U S A 111:7185-7190.

Bosher SK, Warren RL (1978) Very low calcium content of cochlear endolymph, an extracellular fluid. Nature 273:377-378.

Bustamante C, Marko JF, Siggia ED, Smith S (1994) Entropic elasticity of lambda-phage DNA. Science 265:1599-1599.

Cheung EL, Corey DP (2006) Ca2+ changes the force sensitivity of the hair-cell transduction channel. Biophysical journal 90:124-139.

Corey DP, Hudspeth AJ (1983) Kinetics of the receptor current in bullfrog saccular hair cells. J Neurosci 3:962-976.

788 Corns LF, Johnson SL, Kros CJ, Marcotti W (2014) Calcium entry into stereocilia drives adaptation of
789 the mechanoelectrical transducer current of mammalian cochlear hair cells. Proc Natl Acad Sci U S
790 A 111:14918-14923.

791 Eatock RA (2000) Adaptation in hair cells. Annu Rev Neurosci 23:285-314.

792 Effertz T, Becker L, Peng AW, Ricci AJ (2017) Phosphoinositol-4,5-bisphosphate regulates auditory
793 hair cell mechanotransduction channel pore properties and fast adaptation. J Neurosci.

794 Fettiplace R (2006) Active hair bundle movements in auditory hair cells. The Journal of physiology
795 576:29-36.

796 Fettiplace R, Fuchs PA (1999) Mechanisms of hair cell tuning. Annu Rev Physiol 61:809-834.

797 Fettiplace R, Hackney CM (2006) The sensory and motor roles of auditory hair cells. Nat Rev Neurosci
798 7:19-29.

799 Fettiplace R, Kim KX (2014) The physiology of mechanoelectrical transduction channels in hearing.
800 Physiological reviews 94:951-986.

801 Flock A, Strelioff D (1984) Graded and nonlinear mechanical properties of sensory hairs in the
802 mammalian hearing organ. Nature 310:597-599.

803 Freeman DM, Weiss TF (1990) Hydrodynamic analysis of a two-dimensional model for
804 micromechanical resonance of free-standing hair bundles. Hearing research 48:37-67.

805 Frishkopf LS, DeRosier DJ (1983) Mechanical tuning of free-standing stereociliary bundles and
806 frequency analysis in the alligator lizard cochlea. Hearing research 12:393-404.

807 Furness D, Katori Y, Kumar BN, Hackney C (2008) The dimensions and structural attachments of tip
808 links in mammalian cochlear hair cells and the effects of exposure to different levels of
809 extracellular calcium. Neuroscience 154:10-21.

810 Ge J, Elferich J, Goehring A, Zhao H, Schuck P, Gouaux E (2018) Structure of mouse protocadherin 15
811 of the stereocilia tip link in complex with LHFPL5. eLife 7.

812 Géléoc GS, Lennan GW, Richardson GP, Kros CJ (1997) A quantitative comparison of
813 mechanoelectrical transduction in vestibular and auditory hair cells of neonatal mice. Proc R Soc
814 Lond B 264:611-621.

815 Gillespie PG, Muller U (2009) Mechanotransduction by hair cells: models, molecules, and
816 mechanisms. Cell 139:33-44.

817 Greenwood DD (1990) A cochlear frequency-position function for several species—29 years later.
818 The Journal of the Acoustical Society of America 87:2592-2605.

819 Gummer AW, Hemmert W, Zenner HP (1996) Resonant tectorial membrane motion in the inner ear:
820 its crucial role in frequency tuning. Proc Natl Acad Sci USA 93:8727-8732.

821 Hacohen N, Assad J, Smith W, Corey D (1989) Regulation of tension on hair-cell transduction
822 channels: displacement and calcium dependence. Journal of Neuroscience 9:3988-3997.

823 Happel J, Brenner H (2012) Low Reynolds number hydrodynamics: with special applications to
824 particulate media: Springer Science & Business Media.

825 Holton T, Hudspeth AJ (1983) A micromechanical contribution to cochlear tuning and tonotopic
826 organization. Science 222:508-510.

827 Howard J, Hudspeth A (1988) Compliance of the hair bundle associated with gating of
828 mechanoelectrical transduction channels in the bullfrog's saccular hair cell. Neuron 1:189-199.

829 Hudspeth AJ (1989) How the ear's works work. Nature 341:397-404.

830 Hudspeth AJ (2008) Making an effort to listen: mechanical amplification in the ear. Neuron 59:530-
831 545.

832 Hudspeth AJ (2014) Integrating the active process of hair cells with cochlear function. Nature reviews
833 Neuroscience 15:600-614.

834 Hudspeth AJ, Gillespie PG (1994) Pulling springs to tune transduction: adaptation by hair cells.
835 Neuron 12:1-9.

836 Hudspeth AJ, Julicher F, Martin P (2010) A critique of the critical cochlea: Hopf--a bifurcation--is
837 better than none. Journal of neurophysiology 104:1219-1229.

838 Indzhykulian AA, Stepanyan R, Nelina A, Spinelli KJ, Ahmed ZM, Belyantseva IA, Friedman TB, Barr-
839 Gillespie PG, Frolenkov GI (2013) Molecular remodeling of tip links underlies mechanosensory
840 regeneration in auditory hair cells. PLoS biology 11:e1001583.

841 Jaramillo F, Hudspeth AJ (1993) Displacement-clamp measurement of the forces exerted by gating
842 springs in the hair bundle. Proc Natl Acad Sci U S A 90:1330-1334.

843 Johnson SL, Beurg M, Marcotti W, Fettiplace R (2011) Prestin-driven cochlear amplification is not
844 limited by the outer hair cell membrane time constant. Neuron 70:1143-1154.

845 Kachar B, Parakkal M, Kurc M, Zhao Y, Gillespie PG (2000) High-resolution structure of hair-cell tip
846 links. Proc Natl Acad Sci USA 97:13336-13341.

847 Kang H, Wen Q, Janmey PA, Tang JX, Conti E, MacKintosh FC (2009) Nonlinear elasticity of stiff
848 filament networks: strain stiffening, negative normal stress, and filament alignment in fibrin gels.
849 The Journal of Physical Chemistry B 113:3799-3805.

850 Kazmierczak P, Sakaguchi H, Tokita J, Wilson-Kubalek EM, Milligan RA, Muller U, Kachar B (2007)
851 Cadherin 23 and protocadherin 15 interact to form tip-link filaments in sensory hair cells. Nature
852 449:87-91.

853 Kennedy HJ, Crawford AC, Fettiplace R (2005) Force generation by mammalian hair bundles supports
854 a role in cochlear amplification. Nature 433:880-883.

855 Kennedy HJ, Evans MG, Crawford AC, Fettiplace R (2003) Fast adaptation of mechanoelectrical
856 transducer channels in mammalian cochlear hair cells. Nat Neurosci 6:832-836.

857 Kennedy HJ, Evans MG, Crawford AC, Fettiplace R (2006) Depolarization of cochlear outer hair cells
858 evokes active hair bundle motion by two mechanisms. Journal of Neuroscience 26:2757-2766.

859 Kim KX, Fettiplace R (2013) Developmental changes in the cochlear hair cell mechanotransducer
860 channel and their regulation by transmembrane channel–like proteins. The Journal of general
861 physiology 141:141-148.

862 Kozlov AS, Risler T, Hudspeth A (2007) Coherent motion of stereocilia assures the concerted gating of
863 hair-cell transduction channels. Nature neuroscience 10:87.

864 Kozlov AS, Baumgart J, Risler T, Versteegh CP, Hudspeth A (2011) Forces between clustered
865 stereocilia minimize friction in the ear on a subnanometre scale. Nature 474:376.

866 Kros CJ, Rusch A, Richardson GP (1992) Mechano-electrical transducer currents in hair cells of the
867 cultured neonatal mouse cochlea. Proceedings Biological sciences / The Royal Society 249:185-
868 193.

869 Leith D (1987) Drag on Nonspherical Objects. Aerosol Science and Technology 6:153-161.

870 Lewis ER, Leverenz EL, Koyama H (1982) The tonotopic organization of the bullfrog amphibian papilla,
871 an auditory organ lacking a basilar membrane. Journal of comparative physiology 145:437-445.

872 Lim DJ (1986) Functional structure of the organ of Corti: a review. Hear Res 22:117-146.

873 Manley GA, Yates GK, Köppl C (1988) Auditory peripheral tuning: evidence for a simple resonance
874 phenomenon in the lizard Tiliqua. Hearing research 33:181-189.

875 Markin VS, Hudspeth AJ (1995) Gating-spring models of mechanoelectrical transduction by hair cells
876 of the internal ear. Annu Rev Biophys Biomol Struct 24:59-83.

877 Marquis RE, Hudspeth AJ (1997) Effects of extracellular Ca2+ concentration on hair-bundle stiffness
878 and gating-spring integrity in hair cells. Proc Natl Acad Sci USA 94:11923-11928.

879 Martin P (2008) Active hair-bundle motility of the hair cells of vestibular and auditory organs. In:
880 Active processes and otoacoustic emissions in hearing (Manley GA, Popper AN, Fay RR, eds), pp
881 93-143. New York: Springer.

882 Martin P, Mehta A, Hudspeth A (2000) Negative hair-bundle stiffness betrays a mechanism for
883 mechanical amplification by the hair cell. Proceedings of the national academy of sciences
884 97:12026-12031.

885 Martin P, Hudspeth AJ, Jülicher F (2001) Comparison of a hair bundle's spontaneous oscillations with
886 its response to mechanical stimulation reveals the underlying active process. Proc Natl Acad Sci
887 USA 98:14380-14385.

888 Martin P, Bozovic D, Choe Y, Hudspeth A (2003) Spontaneous oscillation by hair bundles of the
889 bullfrog's sacculus. Journal of Neuroscience 23:4533-4548.

890 Meaud J, Grosh K (2011) Coupling active hair bundle mechanics, fast adaptation, and somatic motility
891 in a cochlear model. Biophysical journal 100:2576-2585.

892 Michalski N, Petit C (2015) Genetics of auditory mechano-electrical transduction. Pflügers Archiv-
893 European Journal of Physiology 467:49-72.

894 Neveu A (2009) Suitability of European green frogs for intensive culture: Comparison between
895 different phenotypes of the esculenta hybridogenetic complex. Aquaculture 295:30-37.

896 Nobili R, Mammano F (1996) Biophysics of the cochlea II: Stationary nonlinear phenomenology. The
897 Journal of the Acoustical Society of America 99:2244-2255.

898 Ó Maoiléidigh D, Jülicher F (2010) The interplay between active hair bundle motility and
899 electromotility in the cochlea. The Journal of the Acoustical Society of America 128:1175-1190.

900 Pan B, Akyuz N, Liu X-P, Asai Y, Nist-Lund C, Kurima K, Derfler BH, György B, Limapichat W, Walujkar S
901 (2018) TMC1 forms the pore of mechanosensory transduction channels in vertebrate inner ear
902 hair cells. Neuron 99:736-753. e736.

903 Peng AW, Effertz T, Ricci AJ (2013) Adaptation of mammalian auditory hair cell mechanotransduction
904 is independent of calcium entry. Neuron 80:960-972.

905 Peng AW, Gnanasambandam R, Sachs F, Ricci AJ (2016) Adaptation Independent Modulation of
906 Auditory Hair Cell Mechanotransduction Channel Open Probability Implicates a Role for the Lipid
907 Bilayer. J Neurosci 36:2945-2956.

908 Peng AW, Belyantseva IA, Hsu PD, Friedman TB, Heller S (2009) Twinfilin 2 regulates actin filament
909 lengths in cochlear stereocilia. Journal of Neuroscience 29:15083-15088.

910 Pickles J, Comis S, Osborne M (1984) Cross-links between stereocilia in the guinea pig organ of Corti,
911 and their possible relation to sensory transduction. Hearing research 15:103-112.

912 Pickles J, Osborne M, Comis S (1987) Vulnerability of tip links between stereocilia to acoustic trauma
913 in the guinea pig. Hearing research 25:173-183.

914 Powers RJ, Roy S, Atilgan E, Brownell WE, Sun SX, Gillespie PG, Spector AA (2012) Stereocilia
915 membrane deformation: implications for the gating spring and mechanotransduction channel.
916 Biophysical journal 102:201-210.

917 Reichenbach T, Hudspeth AJ (2014) The physics of hearing: fluid mechanics and the active process of
918 the inner ear. Reports on progress in physics Physical Society 77:076601.

919 Ricci A, Crawford A, Fettiplace R (2002) Mechanisms of active hair bundle motion in auditory hair
920 cells. Journal of Neuroscience 22:44-52.

921 Ricci AJ, Wu YC, Fettiplace R (1998) The endogenous calcium buffer and the time course of
922 transducer adaptation in auditory hair cells. J Neurosci 18:8261-8277.

923 Ricci AJ, Crawford AC, Fettiplace R (2003) Tonotopic variation in the conductance of the hair cell
924 mechanotransducer channel. Neuron 40:983-990.

925 Ricci AJ, Kennedy HJ, Crawford AC, Fettiplace R (2005) The transduction channel filter in auditory hair
926 cells. J Neurosci 25:7831-7839.

927 Rief M, Gautel M, Oesterhelt F, Fernandez JM, Gaub HE (1997) Reversible unfolding of individual titin
928 immunoglobulin domains by AFM. science 276:1109-1112.

929 Roth B, Bruns V (1992) Postnatal development of the rat organ of Corti. II. Hair cell receptors and
930 their supporting elements. Anat Embryol 185:571-581.

Russell I, Sellick P (1983) Low-frequency characteristics of intracellularly recorded receptor potentials in guinea-pig cochlear hair cells. The Journal of Physiology 338:179-206.

Russell IJ, Kössl M, Richardson GP (1992) Nonlinear mechanical responses of mouse cochlear hair bundles. Proc R Soc Lond B 250:217-227.

Schlichting VH (1933) Laminare strahlausbreitung. ZAMM-Journal of Applied Mathematics and Mechanics/Zeitschrift für Angewandte Mathematik und Mechanik 13:260-263.

Sotomayor M, Weihofen WA, Gaudet R, Corey DP (2010) Structural determinants of cadherin-23 function in hearing and deafness. Neuron 66:85-100.

Tilney LG, Tilney MS (1988) The actin filament content of hair cells of the bird cochlea is nearly constant even though the length, width, and number of stereocilia vary depending on the hair cell location. The Journal of cell biology 107:2563-2574.

Tilney LG, Tilney MS, DeRosier DJ (1992) Actin filaments, stereocilia, and hair cells: how cells count and measure. Annual review of cell biology 8:257-274.

Tinevez JY, Julicher F, Martin P (2007) Unifying the various incarnations of active hair-bundle motility by the vertebrate hair cell. Biophysical journal 93:4053-4067.

Tirado MM, Torre JGdl (1979) Translational friction coefficients of rigid, symmetric top macromolecules. Application to circular cylinders. The Journal of Chemical Physics 71:2581-2587.

Turner RG, Muraski AA, Nielsen DW (1981) Cilium length: influence on neural tonotopic organization. Science.

Viberg A, Canlon B (2004) The guide to plotting a cochleogram. Hear Res 197:1-10.

Vilfan A, Duke T (2003) Two adaptation processes in auditory hair cells together can provide an active amplifier. Biophysical journal 85:191-203.

Von Békésy G, Wever EG (1960) Experiments in hearing: McGraw-Hill New York.

Waguespack J, Salles FT, Kachar B, Ricci AJ (2007) Stepwise morphological and functional maturation of mechanotransduction in rat outer hair cells. J Neurosci 27:13890-13902.

Wright A (1984) Dimensions of the cochlear stereocilia in man and the guinea pig. Hear Res 13:89-98.

FIGURES

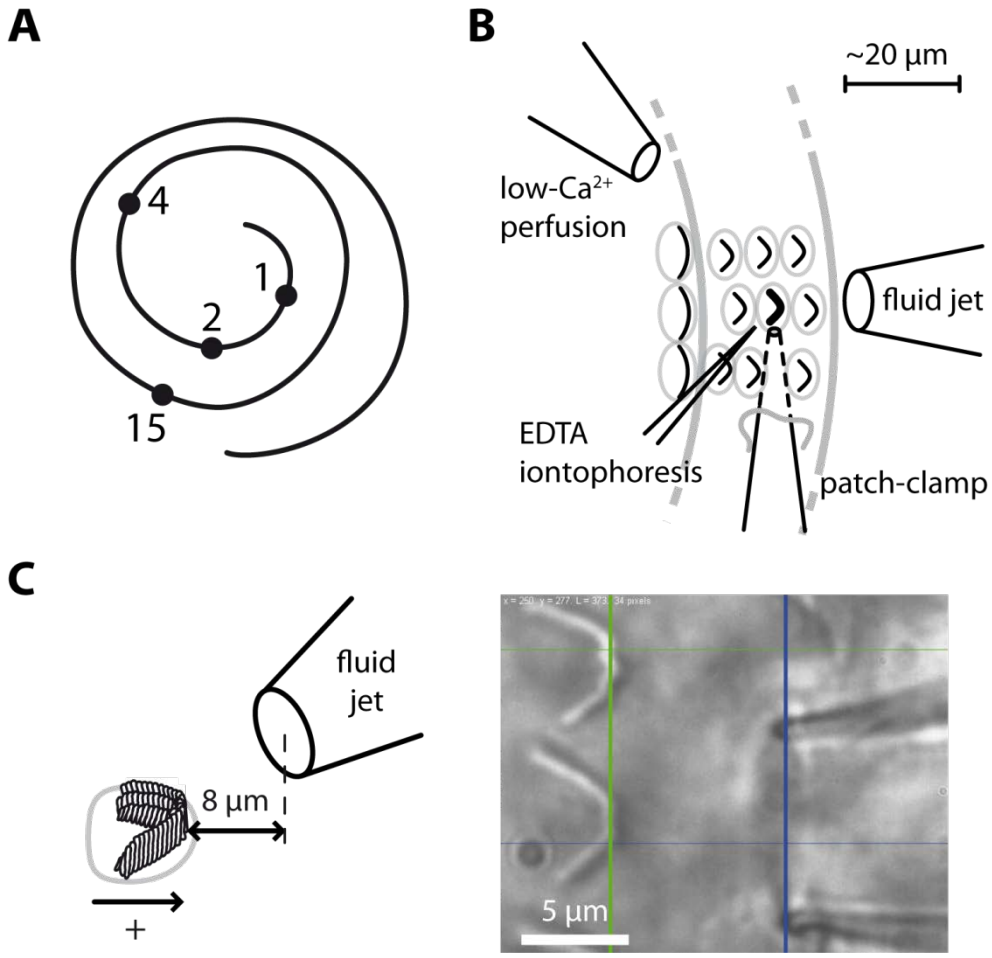

Figure 1: Hair-bundle stimulation along the tonotopic axis of the rat cochlea.

(A) Schematic representation of the tonotopic axis of the rat cochlea. Recordings were made at locations marked by black disks, corresponding to characteristic frequencies (in kHz) increasing from the apex to the base of the cochlea as indicated on the figure and to fractional distances from the apex of 5%, 10%, 20%, and 50%. The rat cochlea was typically 10 mm long. Adapted from (Viberg and Canlon, 2004). **(B)** Schematic layout of the experimental pipettes around a given outer hair cell. We combined fluid-jet stimulation of single hair bundles, iontophoresis of a Ca^{2+} chelator (EDTA), patch-clamp recordings of transduction currents, and perfusion of low-Ca^{2+} saline. **(C)** Schematic representation of the fluid-jet pipette and of a hair bundle (left) and micrograph of a fluid-jet pipette ready to stimulate an outer hair cell of the rat cochlea (right). A positive (negative) deflection of the hair bundle, as defined on the drawing, was elicited by fluid suction (ejection) into (from) the pipette, promoting opening (closure) of the transduction channels. The horizontal projected distance

between the mouth of the pipette (blue vertical line) and the hair bundle (green vertical line) was set at ~8 µm.

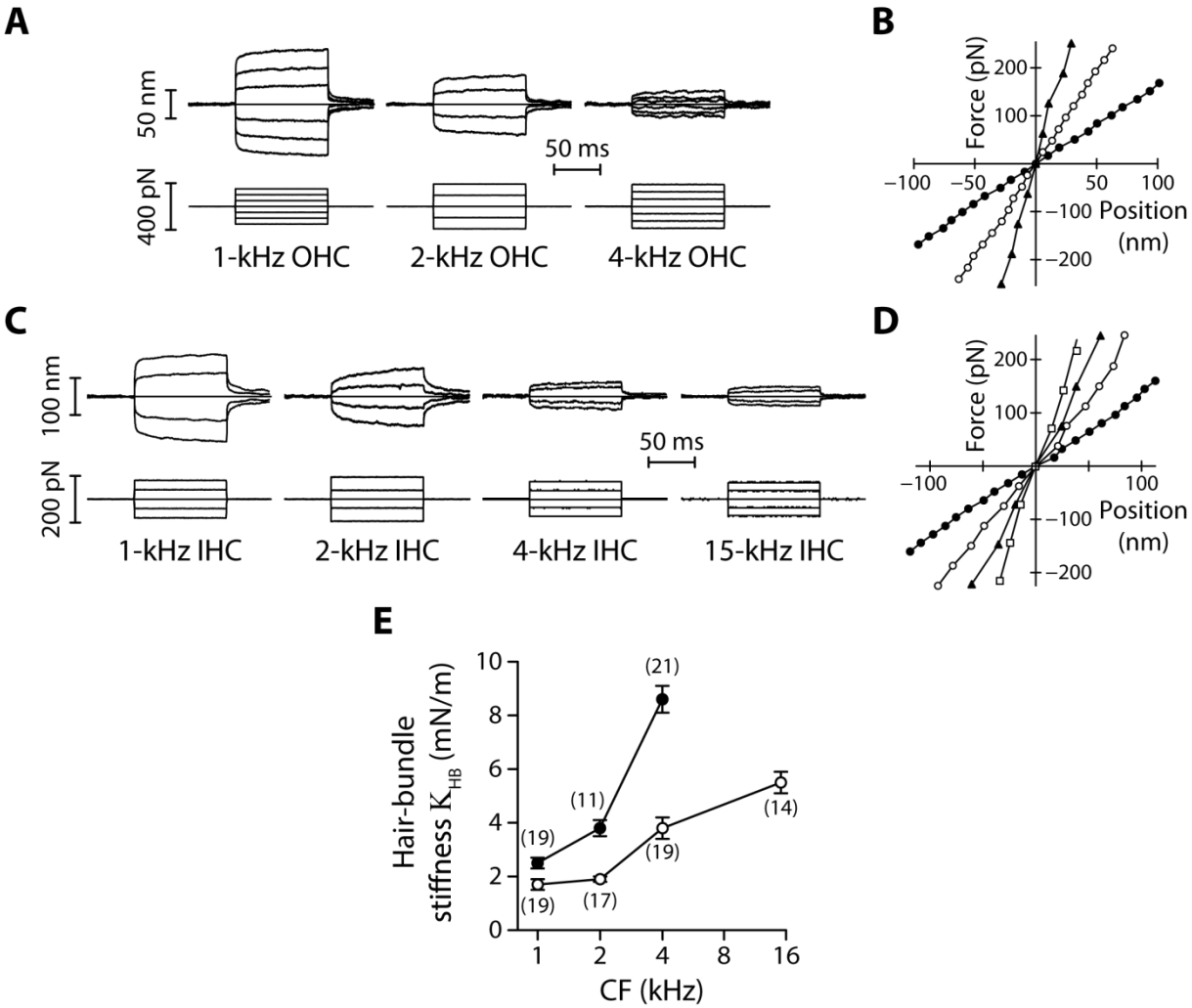

FIGURE 2: Stiffness gradients of the hair bundle.

(A) Hair-bundle movements (top) in response to series of force steps (bottom) for outer hair cells (OHC) with characteristic frequencies of 1, 2 and 4 kHz (from left to right). **(B)** Force-displacement relations for the data shown in **A**, with black disks, white disks and black triangles corresponding to characteristic frequencies of 1, 2 and 4 kHz, respectively. **(C)** Hair-bundle movements (top) in response to series of force steps (bottom) for inner hair cells (IHC) with characteristic frequencies of 1, 2, 4, and 15 kHz. **(D)** Force-displacement relations for the data shown in **C**, with black disks, white disks, black triangles, and white squares corresponding to characteristic frequencies of 1, 2, 4, and 15 kHz, respectively. **(E)** Stiffness (K_{HB}) of a hair bundle under control conditions as a function of the characteristic frequency (CF) for inner (white disks) and outer (black disks) hair cells. Each data point in **E** is the mean ± standard error of the mean (SEM) with the number of cells indicated between brackets.

The following source data is available for figure 2:

Source data 1. Statistical significance.

Source data 2. Hair-bundle stiffness of inner and outer hair cells as a function of the characteristic frequency.

The following figure supplements are available for figure 2:

Figure supplement 1. Velocity field of a fluid jet.

Figure supplement 2. Geometrical characteristics of a fluid jet.

Figure supplement 3. Rise time and linearity of the fluid-jet stimulus.

Figure supplement 4. Test of fluid-jet calibration in the frog's sacculus.

Figure Supplement 5. Mechanical creep during a force step.

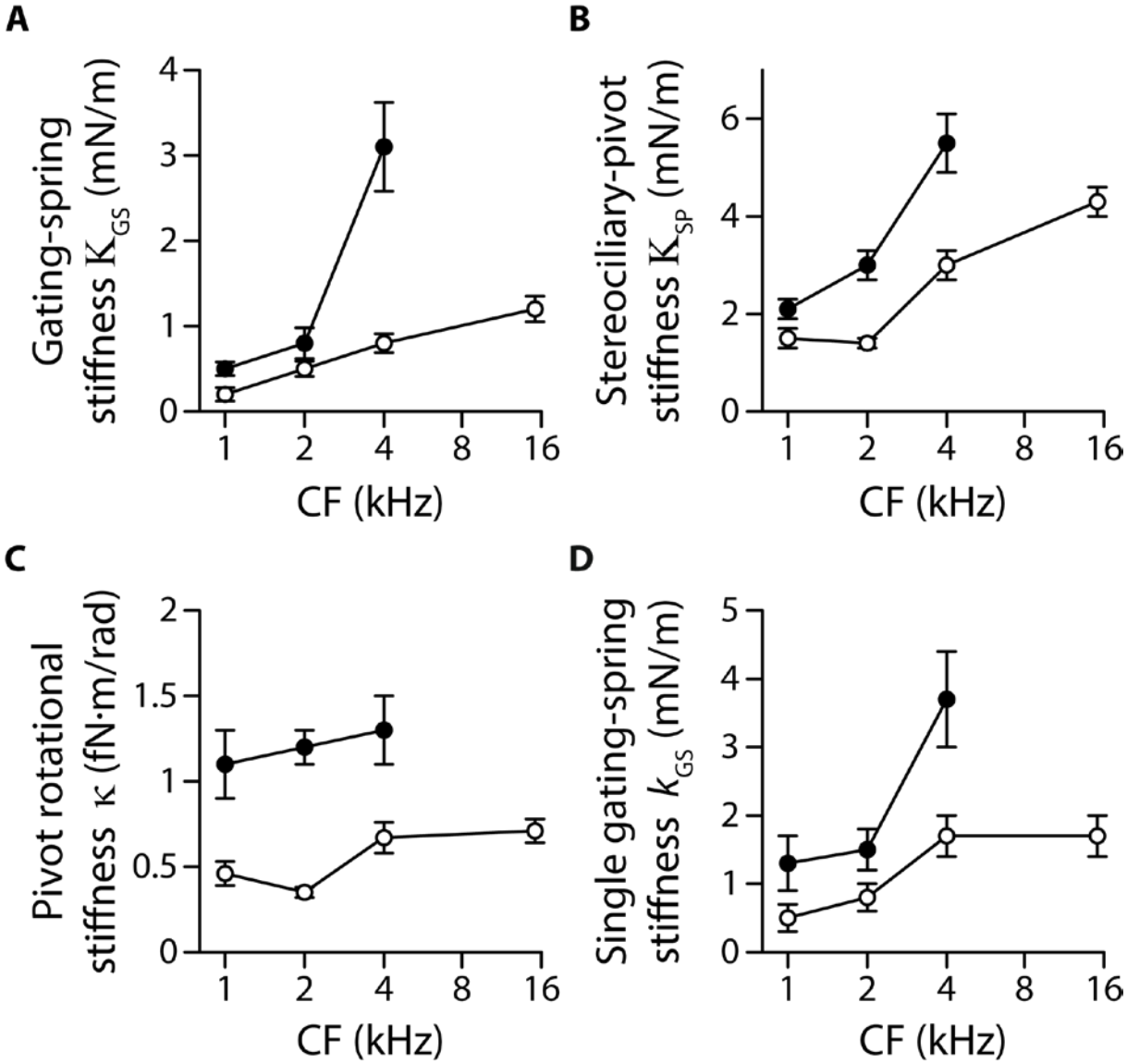

FIGURE 3: Stiffness gradients of the gating springs and of the stereociliary pivots. Stiffness **(A)** of the contribution of the gating springs ($K_{GS} = r\,K_{HB}$), **(B)** of a hair bundle after tip-link disruption, corresponding to the contribution of the stereociliary pivots ($K_{SP} = (1-r)\,K_{HB}$), **(C)** of a single stereociliary pivot ($\kappa = K_{SP}\,h^2/N_{SP}$), and **(D)** of a single gating spring ($k_{GS} = K_{GS}\,\gamma^2/N_{TL}$) as a function of the characteristic frequency (CF) for inner (white disks) and outer (black disks) hair cells. These stiffnesses were calculated from measured values of the hair-bundle stiffness K_{HB} (Fig. 2), the amplitude ratio $1-r$ of hair-bundle movements before and after tip-link disruption (Figure 3–figure supplement 1), the hair-bundle height h and the number of stereocilia N_{SP} (Figure 3-figure supplement 2), and the average number N_{TL} of intact tip links (Figure 3–figure supplement 3). Each data point is the mean ± SEM; SEMs were calculated as described in the Methods.

The following source data is available for figure 3:

Source data 1. Morphological parameters of inner and outer hair-cell bundles.

Source data 2. Statistical significance.

Source data 3. Gating-spring contribution to the hair-bundle stiffness.

Source data 4. Hair-bundle morphology along the tonotopic axis.

Source data 5. Transduction currents and number of intact tip links along the tonotopic axis.

The following figure supplements are available for figure 3:

Figure supplement 1. Gating-spring contribution to the hair-bundle stiffness.

Figure supplement 2. Hair-bundle morphology along the tonotopic axis.

Figure supplement 3. Transduction currents and number of intact tip links along the tonotopic axis.

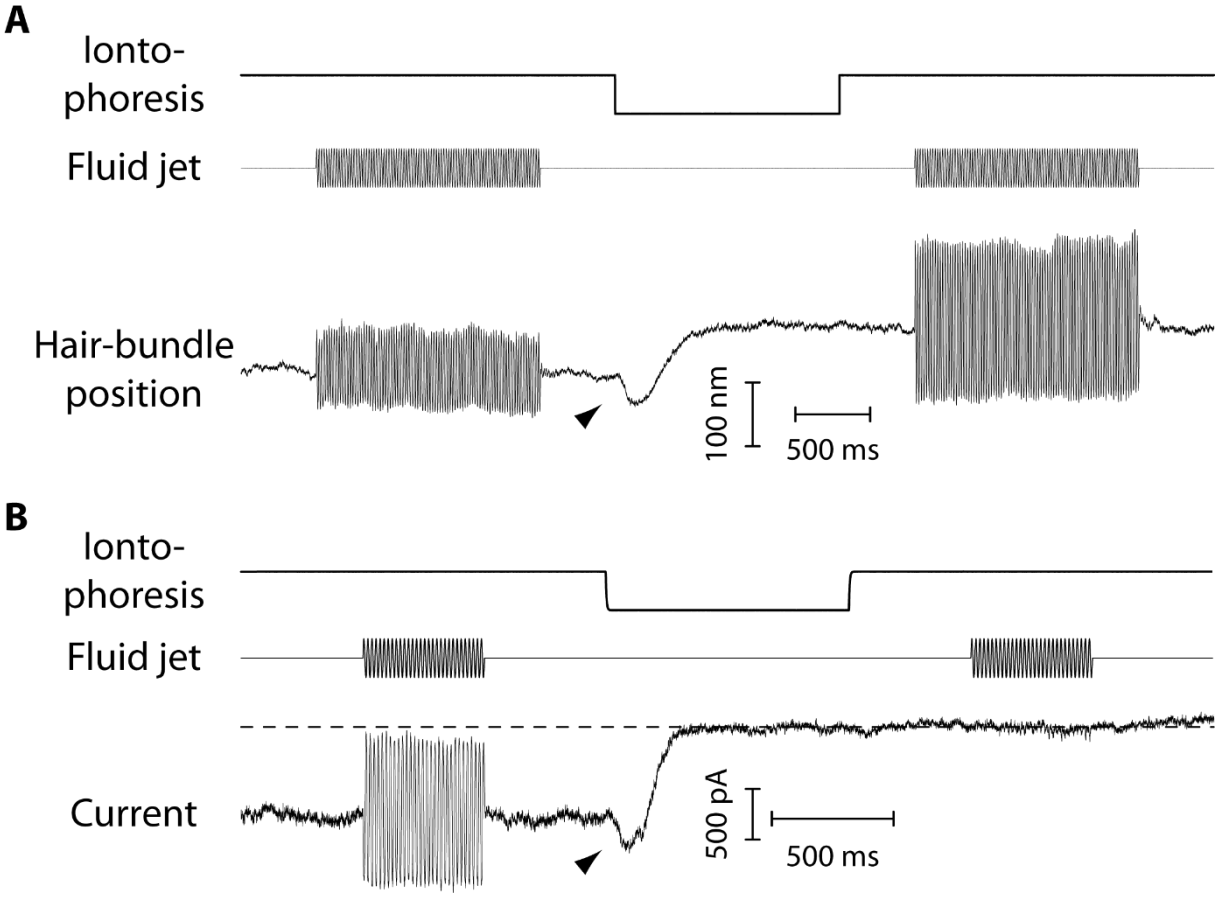

FIGURE 4: Mechanical and electrical response of a hair bundle to fluid-jet stimulation and fast calcium chelation.

(A) An iontophoretic step of a calcium chelator (EDTA; top) elicited a biphasic movement of the hair bundle from an inner hair cell (bottom): the hair bundle first moved in the negative direction (arrow head) and then in the positive direction. After iontophoresis, the position baseline was offset by $\Delta X_{\mathrm{R}} = +78$ nm with respect to the resting position at the start of the experiment. A sinusoidal command to a fluid jet (middle) evoked hair-bundle movements (bottom) that increased in magnitude, here by 50%, after application of the iontophoretic step. Repeating the iontophoretic step elicited no further movement and the response to fluid-jet stimulation remained of the same magnitude. A similar behaviour was observed with 101 inner and 44 outer hair cells. **(B)** An iontophoretic step of EDTA (top) also elicited biphasic variations of the transduction current: the inward current first increased (arrow head) and then decreased. Before application of the calcium chelator, fluid-jet stimulation evoked a transduction current of 1.5-nA peak-to-peak magnitude; the open probability of the transduction channels was near ½. The transduction current was abolished by the iontophoretic step. Outer hair cell at the 4-kHz location; the same behaviour was observed

with 17 outer hair cells. In **A**-**B**, the command signal to the fluid-jet device was a 60-Hz sinusoid and we applied a −100-nA iontophoretic step on top of a +10-nA holding current. The hair bundles were exposed to 20-μM Ca^{2+}. In **B**, the dashed line indicates the current for which the transduction channels are all closed.

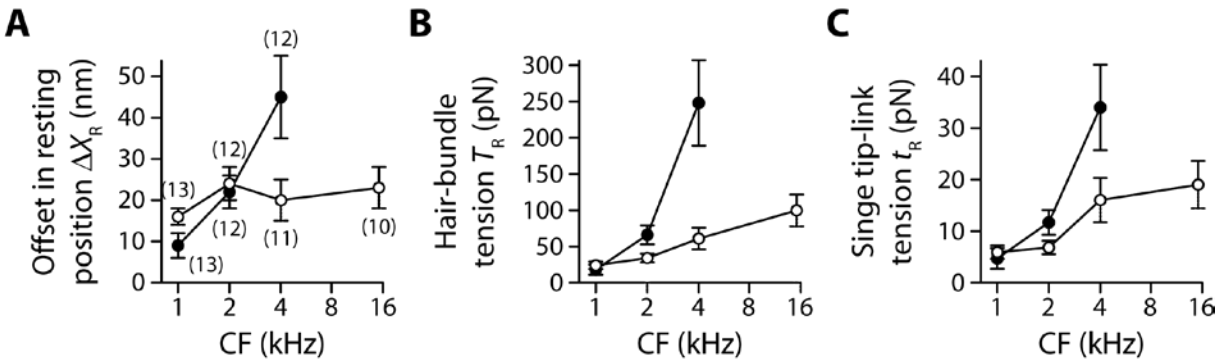

FIGURE 5: Gradients in tip-link tension at rest.

Offset ΔX_{R} in the resting position of a hair bundle resulting from tension release in the tip links **(A)**, tip-link tension $T_{\mathrm{R}} = \mathrm{K_{SP}}\ \Delta X_{\mathrm{R}}$ in the hair bundle **(B)** and tension $t_{\mathrm{R}} = T_{\mathrm{R}}/(\gamma\ N_{TL})$ along the oblique axis of a single tip link **(C)** as a function of the characteristic frequency (CF) for inner (white disks) and outer (black disks) hair cells. The hair-bundle tension T_{R} **(B)** was calculated as the product of the stereociliary-pivot stiffness $\mathrm{K_{SP}}$ shown in Fig. 3B and the data shown in **A**; this tension is estimated along the bundle's horizontal axis of mirror symmetry. The single tip-link tension t_{R} was then deduced from the projection factor γ and the average number N_{TL} of intact tip links in a hair bundle (Figure 3–figure supplement 3). Each data point in **A** is the mean ± SEM with the number of cells indicated between brackets; in **B-C**, mean values and SEMs were calculated as described in the Methods.

The following source data is available for figure 5:

Source data 1. Statistical significance.

Source data 2. Offset in the resting position of a hair bundle upon tip-link disruption.

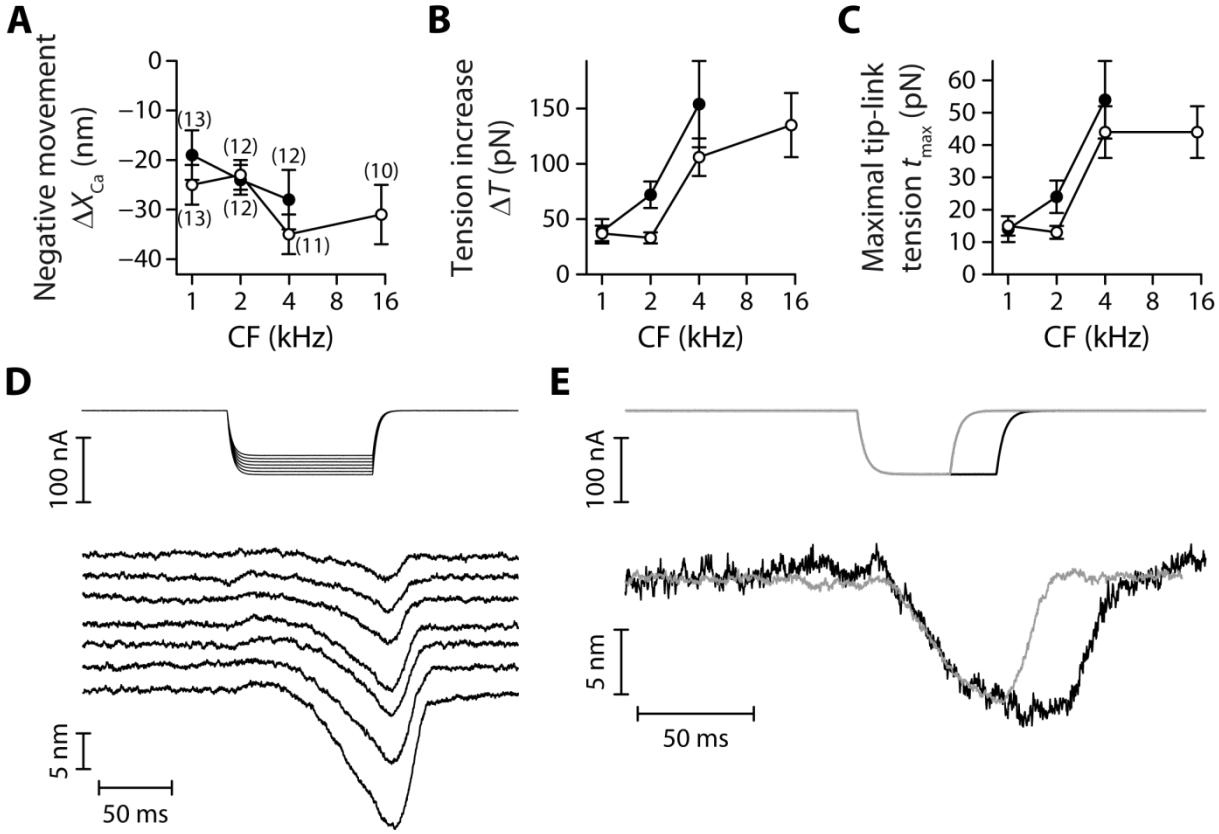

FIGURE 6: Tensioning of the tip links at decreased Ca^{2+} concentrations.

The amplitude of the negative hair-bundle movement ΔX_{Ca} **(A)**, of the maximal increase $\Delta T = -\mathrm{K_{SP}}\,\Delta X_{\mathrm{Ca}}$ in hair-bundle tension **(B)**, and of the maximal tension $t_{\max} = t_R + \Delta T/(\gamma\, N_{TL})$ in a single tip link **(C)** are plotted as a function of the hair cell's characteristic frequency (CF). The tension increase in **B** was calculated from the stiffness $\mathrm{K_{SP}}$ of the stereociliary pivots (Fig. 3B) and the data shown in **A**. The single tip-link tension $t_{\max}$ was then deduced from the tension at rest t_R in a single tip link (Fig. 5C), the projection factor γ (Figure 3–figure supplement 2) and the average number N_{TL} of intact tip links (Figure 3–figure supplement 3). **(D)** Current-step commands (top) applied to an iontophoretic pipette containing the Ca^{2+} chelator EDTA evoked reversible negative movements of the hair bundle (bottom). **(E)** When the stimulus (top) was long enough, the hair bundle position could reach a steady state (bottom), corresponding to higher resting tension in the tip links. In **A-C**, the hair bundles were immersed in low-Ca^{2+} saline, for which EDTA iontophoresis led to tip-link disruption. Positions and tensions were estimated at the point of polarity reversal of the hair-bundle movement (see Fig. 4A), thus at the initiation of tip-link disruption, where the hair bundle reached its largest deflection in the negative direction and tension was thus maximal. Black and white disks correspond to outer and inner hair cells, respectively. The error bars in **A** represent ±SEM with numbers of cells indicated between brackets; in **B-C**,

mean values and SEMs were calculated as described in the Methods. In **D-E**, the hair bundles were immersed in a saline containing 500-μM Ca^{2+}; this higher Ca^{2+} concentration preserved the integrity of the tip links upon EDTA iontophoresis.

The following source data is available for figure 6:

Source data 1. Statistical significance.

Source data 2. Negative movement ΔX_{Ca} of the hair-bundle before tip-link disruption.

1093